NITROUS OXIDE BIOGEOCHEMISTRY IN THE NORTHERN GULF OF MEXICO

An Undergraduate Research Scholars Thesis

by

HUNTER ADAMS

Submitted to the LAUNCH: Undergraduate Research office at
Texas A&M University
in partial fulfillment of requirements for the designation as an

UNDERGRADUATE RESEARCH SCHOLAR

Approved by
Faculty Research Advisor: Dr. Shari Yvon-Lewis

May 2022

Major: Oceanography

RESEARCH COMPLIANCE CERTIFICATION

Research activities involving the use of human subjects, vertebrate animals, and/or biohazards must be reviewed and approved by the appropriate Texas A&M University regulatory research committee (i.e., IRB, IACUC, IBC) before the activity can commence. This requirement applies to activities conducted at Texas A&M and to activities conducted at non-Texas A&M facilities or institutions. In both cases, students are responsible for working with the relevant Texas A&M research compliance program to ensure and document that all Texas A&M compliance obligations are met before the study begins.

I, Hunter Adams, certify that all research compliance requirements related to this Undergraduate Research Scholars thesis have been addressed with my Research Faculty Advisor prior to the collection of any data used in this final thesis submission.

This project did not require approval from the Texas A&M University Research Compliance & Biosafety office.

TABLE OF CONTENTS

ABSTRACT

Nitrous Oxide Biogeochemistry in the Northern Gulf of Mexico

Hunter Adams
Department of Oceanography
Texas A&M University

Research Faculty Advisor: Dr. Shari Yvon-Lewis
Department of Oceanography
Texas A&M University

Nitrous oxide (N_2O) is a potent greenhouse and ozone-depleting gas produced in the ocean and released to the atmosphere. N_2O can be produced in areas of low oxygen such as hypoxic areas and oxygen minimum zones. The shelf region of the northern Gulf of Mexico (GOM) experiences seasonal coastal hypoxia, and the north central GOM has an oxygen minimum layer at about a depth of 500 m. *In-situ* water samples from the northern Gulf of Mexico near the Deepwater Horizon oil spill site were collected and analyzed as part of the 2019 and 2021 Schade Cruises. The sample data is used to better understand the trends in the biogeochemistry and concentration of N_2O in the Gulf of Mexico and to begin the timeseries of Schade Cruise N_2O data. Results showed that N_2O concentrations were ~1.7x higher in 2021 while Mississippi River discharge and nutrient loadings were ~ 2x and 1.5x times lower respectively. Differences in total *in-situ* nutrient concentrations and dissolved oxygen between 2019 and 2021 were negligible. The results illustrate the need for more consistent data from future cruises in order to accurately determine trends in N_2O biogeochemistry in the northern GOM.

ACKNOWLEDGEMENTS

Contributors

I would like to thank my amazing faculty advisor, Dr. Shari Yvon-Lewis, for their wisdom, guidance, and patience throughout the course of this research.

Thanks also go to Veronica Burgos and Melissa Shugart for their assistance in processing samples.

Funding Sources

Publication supported in part by an Institutional Grant NA18OAR4170088, to the Texas Sea Grant College Program from the National Sea Grant Office, National Oceanic and Atmospheric Administration, U.S. Department of Commerce.

NOMENCLATURE

CTD	Conductivity, temperature, and depth electronics package
GC	Gas Chromatograph
ECD	Electron Capture Detector
OMZ	Oxygen Minimum Zone
ppb	parts per billion
uCO_2	Carbon Dioxide
CH_4	Methane
N_2O	Nitrous Oxide
NO_2^-	Nitrite
NO_3^-	Nitrate
NH_3	Ammonia
NH_4^+	Ammonium
NO	Nitric Oxide
N_2	Dinitrogen
USGS	U.S. Geological Survey

1. INTRODUCTION

Nitrous oxide (N_2O) is a strong and long-lived greenhouse gas and one of the most potent ozone depleting agents produced from anthropogenic and natural sources. N_2O is 298 times more powerful than carbon dioxide (CO_2) and 12 times more powerful than methane (CH_4) as an atmospheric warmer in units of 100-year global warming potential (GWP). N_2O also has an atmospheric lifetime of approximately 114 years classifying it as a relatively long-lasting gas when compared to gasses such as CH_4 which has a lifetime of 12 years [*IPCC,* 2007]. Now and into the future, it is the most prominent stratospheric ozone depleting gas even when accounting for interference from increasing CH_4 and CO_2 atmospheric concentrations [*Portmann et al.*, 2012; *Revell et al.,* 2015].

The tropospheric abundance of N_2O has increased from 270 to 331 parts per billion (ppb) between 1750 and 2018 due to the increased emissions of N_2O from various sources [*Battle et al.,* 1996; *Denman et al.*, 2007; *Machida et al.,* 1995]. Currently, agriculture is the leading reason why N_2O emissions are increasing over time [Syakila and Kroeze, 2011]. Natural sources from soils and the ocean account for ~57% of total N_2O emissions and anthropogenic sources account for ~43% during 2007 to 2016. Natural soils and oceans can account for ~58% and ~35% of natural sources respectively from this same time period. Other sources of N_2O include fossil fuel burning, biomass burning, lightning and atmospheric production, as well as inland coastal waters [*Tian et al.,* 2020]. The ocean is a major source of N_2O to the atmosphere because it ubiquitously supersaturated with N_2O. N_2O is only removed from the atmosphere when it is absorbed by bacteria in soils, destroyed by ultraviolet radiation, or atmospheric chemical reactions create other nitrogen oxides from N_2O.

Oceans produce N_2O in oxic and sub-oxic conditions primarily through nitrification and denitrification respectively [Ji et al., 2015]. High N_2O effluxes to the atmosphere can occur from sub-oxic water masses such as hypoxic dead zones or oxygen minimum zones (OMZs) as a result of denitrification which occurs primarily under anoxic conditions. OMZs are characterized by a steep oxygen gradient sandwiching nitrite accumulation at a midrange depth indicating anoxic conditions ($[O_2] < 10nM$) and are permanent features of a regions biogeochemical system [Thamdrup et al., 2012]. Hypoxic dead zones are anoxic water masses that form on the seafloor as a result of the respiration of falling detritus typically in coastal regions where there is significant input of nutrients. Hypoxic dead zones are different from OMZs in that they are not permanent additions to an ocean regions biogeochemical system but instead follow a seasonal pattern of formation.

Unfortunately, the degree to which OMZs contribute to total ocean emissions of N_2O is still uncertain due to the expected expansion of their horizontal and vertical extents. This is because there are still uncertainties in the relationship between N_2O and changing O_2 levels, when N_2O switches from production to consumption, and the rate of net N_2O consumption at low O_2 depending on region [Zamora et al., 2012]. Further research will be required in order to accurately understand the contribution of OMZs to atmospheric N_2O emissions. The same concept also applies to hypoxic dead zones. Changes in dead zone extent as a result of climate change driver perturbations has the potential to increase the area of which N_2O is produced. Supplemental information for OMZs can be found in Appendix B.

In soils and the ocean, N_2O is primarily produced as a by-product of the remineralization of organic matter via nitrification and denitrification [*Butterbach-Bahl et al.,* 2013]. Nitrification is the microbial process in which reduced nitrogen compounds (primarily ammonia (NH_3) and

ammonium (NH_4^+)) are oxidized to nitrite (NO_2^-) and then to nitrate (NO_3^-) by ammonia-oxidizing bacteria (equations 1.1 and 1.2). A small fraction of N_2O is released during nitrification when oxidized ammonia is turned into nitrate via nitrite [*Inatomi et al.*, 2019].

$$NH_3 + O_2 \rightarrow NO_2^- + 3H^+ + 2e^- \quad (1.1)$$

$$NO_2^- + H_2O \rightarrow NO_3^- + 2H^+ + 2e^- \quad (1.2)$$

Denitrification is the reduction of nitrate or nitrite to nitric oxide (NO) and nitrous oxide (N_2O) and then subsequently dinitrogen (N_2). Denitrification occurs though some combination of the following half reactions (equations 1.3, 1.4, 1.5, and 1.6). Equation 1.7 is the complete process expressed as a balanced net redox reaction [*R Knowles*, 1982].

$$NO_3^- + 2H^+ + 2e^- \rightarrow NO_2^- + H_2O \quad (1.3)$$

$$NO_2^- + 2H^+ + 2e^- \rightarrow NO + H_2O \quad (1.4)$$

$$2\,NO + 2H^+ + 2e^- \rightarrow N_2O + H_2O \quad (1.5)$$

$$N_2O + 2H^+ + 2e^- \rightarrow N_2 + H_2O \quad (1.6)$$

$$2NO_3^- + 12H^+ + 10e^- \rightarrow N_2 + 6H_2O \quad (1.7)$$

Under aerobic conditions, it is nitrification that produces N_2O and under anaerobic conditions coupled denitrification primarily produces N_2O [*Ji et al.*, 2015; *Martens*, 2005]. The primary limiting factors of nitrification and denitrification in aquatic environments are nitrogen availability and the amount of dissolved oxygen respectively [*R. Knowles*, 1996; *Ward*, 2013]. Anthropogenic changes to the nitrogen cycle can intensify nitrification rates as more nitrogen is transported to the coastal and open ocean by river outflow or atmospheric deposition. Climate change driven perturbations such as the increasing number and area of hypoxic zones/OMZs can also increase the global rate of denitrification [*Diaz*, 2001; *Ji et al.*, 2015]. Increased *in-situ* production of N_2O could result in higher emissions to the atmosphere.

A large area of coastal hypoxia can be found in the northern Gulf of Mexico continental shelf which typically occurs every summer. The Gulf of Mexico is an ocean basin connected to

the Atlantic Ocean by the Florida straits and is surrounded by the United States, Mexico, and Cuban coasts. The gulf is also home to the Loop Current and its continuation the Gulf Stream which provide circulation and nutrient transport for the basin through eddy formation [Oey et al., 2005].The structure and high nutrient loads that come from the Mississippi and Atchafalaya Rivers cause an annual formation of hypoxic water that persists from spring to late summer [*Rabalais et al.*, 2002]. This hypoxic zone has the potential to produce large amounts of N_2O as a result of denitrification and nitrification. This is especially true when considering gulf specific climate change driven perturbations such as potential increased rates of eddy formation, larger and more frequent storm events, and increased hypoxic zone extent. All of these different events can cause increased rates of N_2O emissions to the atmosphere due to water column-mixing and subsequent gas venting to the atmosphere [*Feng et al.*, 2014; *Nevison et al.*, 2004; *J T Walker et al.*, 2010; *N Walker et al.*, 2003].

Using *in-situ* water samples and CTD data from the Northern Gulf of Mexico near the Deepwater Horizon oil spill site from research cruises, trends between N_2O production and climate change events such as those described above could potentially be determined for the northern Gulf of Mexico. The 2019 and 2021 Schade Cruise data provides the initial N_2O data necessary to create a timeseries showing these relationships. The Schade cruises are research cruises designed to educate Texas A&M University Department of Oceanography students in shipboard oceanographic data collection techniques and operations. All cruises occur over a period of four days and the cruise area is focused in the Northern Gulf of Mexico near the Deepwater Horizon oil spill site. They occur annually during the summer with the other goal of creating a timeseries of different oceanographic parameters over multiple years. Having data spanning a large timeseries is useful as it allows researchers to establish trends in data and to

eliminate potential outliers in the data set. The 2020 Schade cruise was cancelled as a result of the COVID-19 pandemic and is a significant hole in the timeseries of currently available Schade data.

These cruises provide a unique opportunity to observe and analyze consistent N_2O data from the Northern gulf. This is because N_2O is typically sampled opportunistically on research cruises and is not typically associated with a continuous annual timeseries. By analyzing N_2O data along with river, nutrient, temperature, salinity, and dissolved oxygen (DO) data, preliminary biogeochemical trends of N_2O can be distinguished despite the currently limited timeseries from the 2019 and 2021 Schade Cruises.

2. METHODS

2.1 Sampling Stations

Water samples and CTD data were collected from two research cruises that sampled in the northern Gulf of Mexico (GOM). These cruises took place from May 23rd to the 26th in 2019 (Schade 2019) and June 1st to the 4th in 2021 (Schade 2021) (Figure 2.1). Both cruises sampled in the region of the Gulf of Mexico near the Deepwater Horizon oil spill site and near the Mississippi River Delta. Both cruises followed tracks that that ranged moved between the continental shelf and the open ocean.

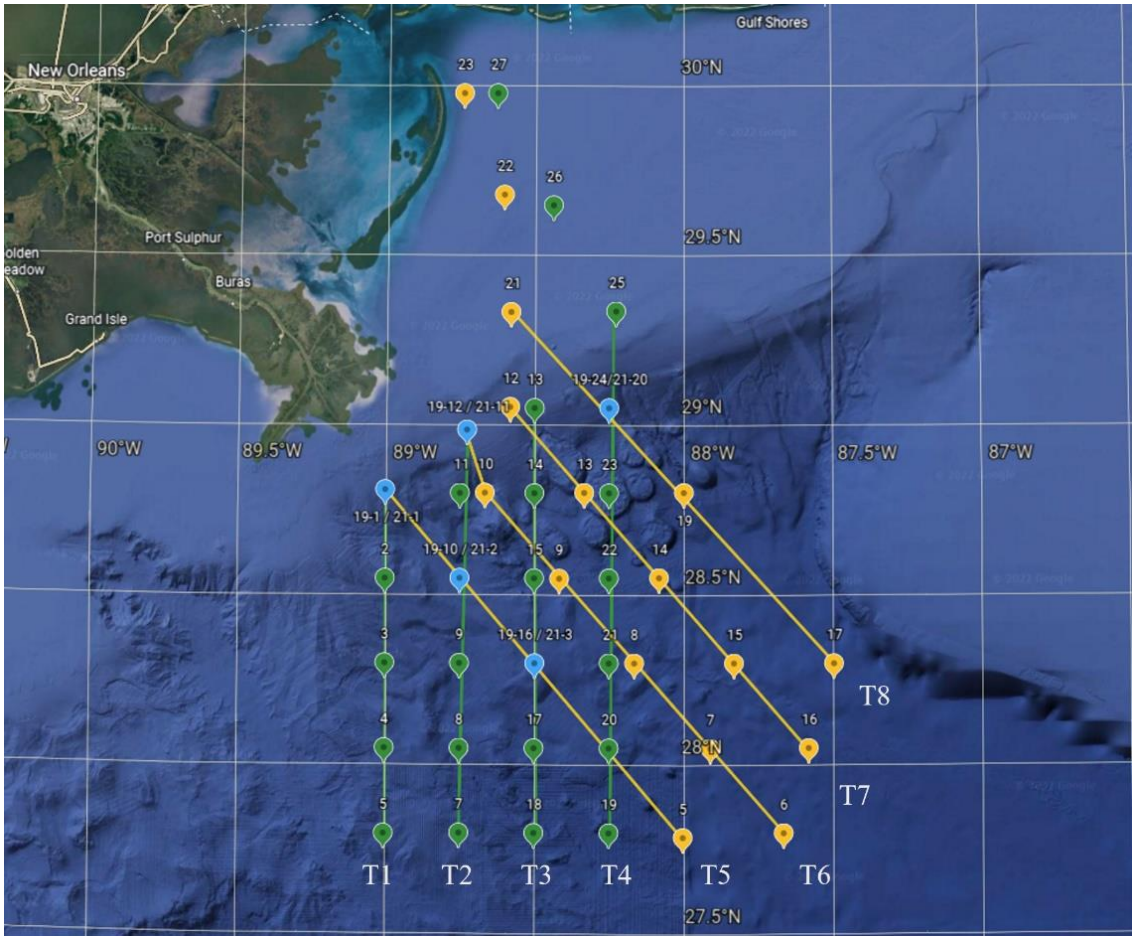

Figure 2.1: Stations and transects of Schade 2019 (green) and Schade 2021 (yellow) cruises. T1, T2, T3, and T4 are the Schade 2019 transects and T5, T6, T7, and T8 are the Schade 2021 transects. The blue stations are stations common to both cruises.

For both cruises, CTD and water sample data were collected from a rosette and an associated set of 12 niskin bottles. Samples were taken at depths ranging between the surface and over 2500 meters deep at different stations. *In-situ* CTD temperature, salinity, and dissolved oxygen concentration data were collected for each cruise and processed after both cruises. Water samples for NH_4^+, NO_2^-, NO_3^-, and N_2O were collected from the rosette niskin bottles. N_2O samples were collected and sealed in 100 mL crimp topped serum bottles. When samples were sealed the meniscus of the water was intact and no atmospheric headspace was introduced. All samples were immediately poisoned with mercuric chloride ($HgCl_2$) to prevent potential degradation due to microbes and were stored in dark insulated boxes. After poisoning, foil tape was used to create a seal on top of the crimp caps in order to prevent any potential gas exchange through the hole created by the needle.

2.2 Nitrous Oxide Analysis

Analysis of all N_2O samples from the 2019 and 2021 Schade cruises were performed at Texas A&M University Department of Oceanography in College Station, TX. Every sample was prepared for analysis by introducing 20 mL of headspace of zero air into each sample bottle. Headspace was created by connecting a 20 mL syringe and a zero air filled Tedlar bag (Sigma-Aldrich, Inc) with an attached needle through the septum and into the top of the sample bottle. The Tedlar bag was used so as to not overpressure the sample bottles. The needle of the syringe reached to the bottom of the bottle and the shorter needle of the Tedlar bag remained near the top of the bottle. The plunger of the syringe was pulled first to create a vacuum that ensured sample water would not enter the tedlar bag. After creating a slight vacuum in the sample bottle, the tedlar bag valve was opened and zero air would enter the sample bottle. When zero air entered the sample bottle freely, the syringe was used to draw 20mL of water from the bottom of the

bottle. This allowed 20 mL of zero air to flow into the bottle and form the appropriate amount of headspace. After drawing out 20 mL of sample water, the valve of the Tedlar bag was closed and the syringe and bag were removed from the sample bottle. The septum on the sample bottle was then taped with foil tape in order to prevent gas exchange through the holes created by the needles. Sample water from the syringe was deposited in a mercuric chloride waste receptacle. After depositing the waste water, the sample bottle was agitated and allowed to rest overnight so that gases dissolved in the water could equilibrate with the headspace. Needles from the syringe and tedlar bag were examined to ensure that there were no blockages in the needle from the material that makes up the crimp cap. After this, the process was repeated for every sample to be analyzed.

After equilibrating overnight, the headspace samples were ready to be analyzed using a gas chromatograph with an electron capture detector (GC/ECD). At the start of each processing day the GC/ECD was baked and junk air samples were injected in order to warm up the instrument. At this time, room temperature was also recorded in order to later determine solubility for the samples. In order to ensure the accuracy of sample data, a calibration curve was created for each day of sample processing and the GC/ECD was run almost continuously. Calibration curves were created using gasses of known N_2O concentration. These standard gasses were stored in air flasks where a syringe was used to collect a gas sample of approximately 10 mL for injection into the GC/ECD. Triplicate samples of three standard gasses and zero air were used to create the calibration curves (Figure 2.2).

After a calibration curve was created, N_2O samples were injected into the GC/ECD and analyzed. Approximately 10 mL of headspace was removed from each sample bottle and injected into the GC/ECD. Headspace was removed by attaching a tedlar bag filled with zero air and a

syringe to the top of the sample bottle. The needle of the tedlar bag remained at the top of the bottle and the needle of the syringe was positioned right above the surface of the sample water. This was done to ensure that sample headspace and not zero air would be collected by the syringe when the plunger was pulled. The valve of the bag was opened and ~10mL of sample headspace was pulled into the syringe. Immediately after drawing in headspace into the syringe the valve of the tedlar bag was closed and the syringe was removed from the bottle. The needle was then separated from the syringe and the sample headspace was injected into the GC/ECD steadily at the appropriate time of injection for the sequence. Barometric pressure in units of millibar (mbar) and GC/ECD loop temperature in units of degrees Celsius (°C) was recorded at the time of injection.

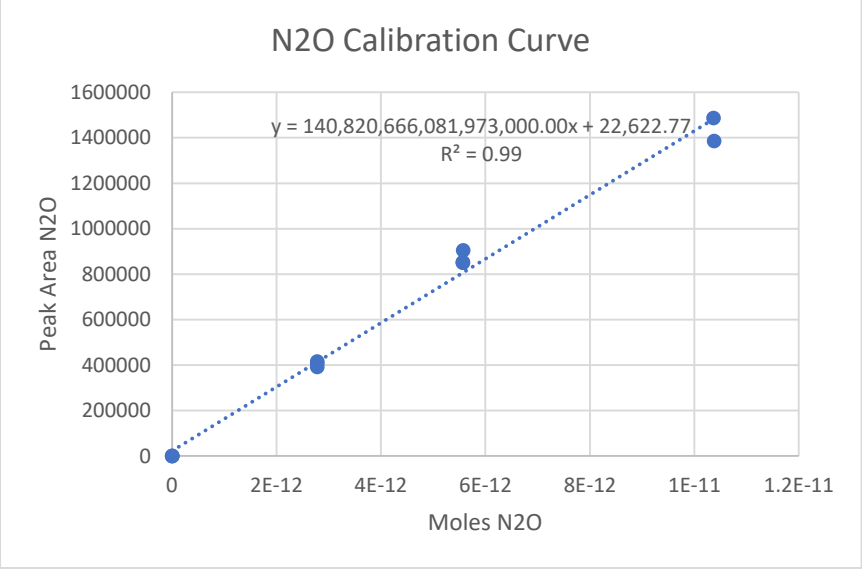

Figure 2.2: A standard calibration curve created from zero air and three gasses of varying but known concentrations of N_2O.

The Ideal Gas Law (equation 2.1) was used to determine the total amount of gas in moles that is present in the GC/ECD loop.

$$PV = nRT \tag{2.1}$$

P is the barometric pressure of the room at the time of sample injection (atm), V is the loop

volume for the GC/ECD equal to 0.0005 L for N_2O, n is the moles of gas in the loop, R is the gas constant equal to 0.08206 L *atm *mol^{-1} *K^{-1}, and T is the loop temperature at the time of sample injection (K). To create the x-axis of the standard curve (moles N_2O), the known concentration of standard gas in units of atmospheres was multiplied by the loop moles of N_2O calculated from the Ideal Gas Law.

To determine the concentration of the bottled samples, the linear regression equation from the standard curve created that same day was used. Y in the equation represents the peak area returned by the GC/ECD corresponding to the different bottle samples. To find the concentration in terms of moles the equation must be solved for x which returns the moles of N_2O in the loop. The N_2O mole fraction, also known as the head space partial pressure (atm), and the mixing ratio (mol*mol^{-1}), was determined by dividing total moles of N_2O calculated from the calibration curve by the total moles of gas in the loop.

N_2O solubility was calculated using equation 2.2:

$$\ln(F) = A_1 + A_2\left(\frac{100}{T}\right) + A_3\ln\left(\frac{T}{100}\right) + A_4\left(\frac{T}{100}\right)^2 + S*\left[B_1 + B_2\left(\frac{T}{100}\right) + B_3\left(\frac{T}{100}\right)^2\right] \qquad (2.2)$$

where, F is the volumetric solubility (mol l^{-1} atm^{-1}), T is the room temperature (K), S is sample salinity (ppt), and A_1, A_2, A_3, A_4, B_1, B_2, and B_3 are gas specific constants [*Sarmiento*, 2013]. The water concentration (mol L^{-1}) of N_2O was calculated by multiplying the volumetric solubility by the partial pressure of N_2O in headspace. The total number of moles in the water can be calculated by multiplying water concentration and volume of water remaining in the sample bottle (L).

Ideal Gas Law was used to determine the moles of N_2O in the headspace. P is the barometric pressure of the room during sample injection (atm), V is the volume of the headspace (~ .02 L), R is the gas constant (0.08206 L*atm*mol^{-1}*K^{-1}), T is the room temperature (K), and n

is the moles of gas in the headspace. Moles of N_2O were found by multiplying the partial pressure by the total moles of gas in the headspace. The water and headspace masses of N_2O are added together and divided by the volume of water (L) to determine the initial concentration of N_2O in the bottle before the headspace was introduced. This result is the true sample concentration.

3. RESULTS AND DISCUSSION

3.1 Surface Analysis

The physical structure of the surface of the Schade 2019 and 2021 cruise areas, characterized by temperature and salinity, showed differences in structure depending on proximity to the coast and Mississippi River Delta (Figures A.1, A.2, A.3, A.4, A.5, A.6, A.7 and A.8). In 2019, stations on top of the continental shelf (stations 25, 26, and 27) had high surface temperatures and low surface salinities compared to the rest of the sampling area (Figures A.1 and A.3). The higher temperatures could have been due to the shallow depths of the region, where there is not as much influence from colder deep water on surface temperature. However, surface temperature distribution from the 2021 Schade Cruise does not support this trend as there was no significant difference in surface temperature distribution between the coastal and open ocean regions (Figure A.4).

The surface salinity between Schade 2019 and 2021 is similar in terms of distribution and value with the only difference being that. Both cruises had lower surface salinities on the continental shelf and higher salinities in the open ocean. The surface salinity distribution between the cruises indicates significant freshwater flux from the coast and the Mississippi River onto the continental shelf especially in 2019. Freshwater flux from rivers and coastal regions typically transports large amounts of nutrients to coastal oceans. Because N_2O is typically limited by nitrogen concentration, it could be assumed that there are high rates of nitrification occurring at or below the ocean surface meaning that there could be high concentrations of N_2O.

Despite higher river discharge and nitrogen loadings in 2019, surface N_2O concentrations were less than in 2021 (Table 3.1). Surface N_2O concentrations were higher in 2021 with an average of 7.95 nM and a standard deviation of 0.41 nM (n=3) from the stations located on the

continental shelf (stations 21, 22, and 23). 2019 Schade stations on the continental shelf (stations 25, 26, and 27) had an average surface N_2O concentration of 3.05 nM and a standard deviation of 1.56 nM (n=3). Stations on the continental shelf were averaged because they are affected by the freshwater flux from the Mississippi River and coast. Both cruises saw elevated concentrations of N_2O on the continental shelf compared to stations near and beyond the continental slope (Figures A.9 and A.10). The inconsistencies in N_2O distribution at the total surface area between cruises could be due to competition between phytoplankton and other microorganisms for nutrients at the surface.

Table 3.1: Average Mississippi River discharge rate (ft^3s^{-1}), mean nitrogen from nitrite combined with nitrate in water (mg L^{-1}), and total nitrogen load for each date range collected from USGS (https://waterdata.usgs.gov/usa/nwis/uv?site_no=07374000).

Date ranges	Average discharge (10^6 ft^3 s^{-1})	Average Nitrogen from NO_3^- plus NO_2^- (10^6 mg L^{-1})	Nitrogen load, metric tons (10^5)
5/23/2019-5/26/2019	1.26	1.46	2.75
5/1/2019 - 6/30/19	1.22	1.45	2.65
6/1/2021-6/4/2021	0.67	1.83	1.84
5/1/2021 - 6/30/21	0.70	1.38	1.44

3.2 Full-depth Range Analysis

Temperature, salinity, and dissolved oxygen (DO) transect heat maps from Schade 2019 and 2021 show that the water column's physical structure between both cruises was similar (Figures A.5, A.6, A.7, A.8, A.11, and A.12). Both cruises had temperature and salinity decrease with depth at a comparable rate and a DO minimum at 500 m. High temperatures at the surface of the water column are due to solar heating and colder, denser, water holding up warmer less dense water. Higher salinities at the surface can be attributed to evaporation. For both cruises, DO concentration decreased with depth until approximately 500 meters and then increased with

depth after this. This is because photosynthesis produces DO at the surface and then microbial respiration lowers its concentration between 250-750 meters when sinking organics from the euphotic zone were oxidized.

NO_3^- concentration trends were the inverse of oxygen concentration trends in 2019 and 2021 and were similar between the cruises (Figures A.11, A.12, A.13, and A.14). This is visible in the transect plots' 250 to 750 meter depth range and comparisons between stations common to both cruises (Figures A.15, A.16, A.17, A.18, and A.19). As oxygen concentration decreased, NO_3^- concentration increased due to the oxidation of sinking organic matter from the euphotic zone and was released back into the water column. NH_4^+ concentrations had no consistent horizontal or vertical trends across transects and cruises (Figures A.20 and A.21).

NO_2^- concentrations and trends were similar between cruises but the distribution was not as uniform in 2021 (Figures A.22 and A.23). In the water column, NO_2^- concentrations generally decreased with increasing depth and had higher concentrations in areas of high DO concentration. This was unexpected, as NO_2^- concentrations usually increase when oxygen concentrations decrease or are low and should have a small maxima where oxygen is decreasing or has a minima in the vertical profiles (Figures A.15, A.16, A.17, A.18, and A.19))[*Ward*, 2013].

N_2O concentrations were expected to mirror the same trends as NO_2^- for Schade 2019 and 2021 as NO_2^- is a primary limiting factor of nitrification in aerobic environments. Unfortunately, in most cases, N_2O concentration trends were the opposite of NO_2^- trends in 2019 and 2021 (Figures A.24 and A.25). Total N_2O concentrations for the 2019 cruise area averaged 4.9 nM with a stand deviation of 2 nM (n = 239). Schade 2021 had an average of 8.2 nM with a standard deviation of 2 nM (n = 206).

A more considerable amount of nutrients, and consequently nitrite, were present from the Mississippi River in 2019; therefore, greater N_2O concentrations were expected for 2021. These limiting nutrients should have fueled nitrification, producing larger amounts of N_2O given that there was no anoxic conditions obsererved. More data from future Schade cruises will be required to make sense of the trends in N2O biogeochemistry.

4. CONCLUSION

In conclusion, results from river, nutrient, and N_2O data reveal the need for a longer timeseries of consistent data from the Northern Gulf of Mexico. Unexpected trends observed from transect heat maps, surface heat maps, and vertical profiles of stations common to both cruises show that the biogeochemical systems of the Norther Gulf of Mexico could be more complex than originally expected. N_2O concentrations in 2021 were greater than in 2019 despite 2019 having almost twice the nutrient loadings from the Mississippi River. The physical structures of both cruises were also similar while nutrient distributions varied significantly further showing the need for more data to compare against. Establishing trends based off of only two years of data is challenging but provides a starting point for future analysis to take place. More data from future Schade Cruises is needed to determine if there is error in the data already collected or to determine new trends.

REFERENCES

Battle, M., et al. (1996), Atmospheric gas concentrations over the past century measured in air from firn at the South Pole, *Nature*, *383*(6597), 231-235, doi:10.1038/383231a0.

Butterbach-Bahl, K., E. M. Baggs, M. Dannenmann, R. Kiese, and S. Zechmeister-Boltenstern (2013), Nitrous oxide emissions from soils: how well do we understand the processes and their controls?, *Philosophical Transactions of the Royal Society B: Biological Sciences*, *368*(1621), 20130122, doi:doi:10.1098/rstb.2013.0122.

Denman, K., et al. (2007), Couplings Between Changes in the Climate System and Biogeochemistry, edited, pp. 499-587.

Diaz, R. (2001), Overview of Hypoxia around the World, *Journal of environmental quality*, *30*, 275-281, doi:10.2134/jeq2001.302275x.

Feng, Y., K. Fennel, G. A. Jackson, S. F. DiMarco, and R. D. Hetland (2014), A model study of the response of hypoxia to upwelling-favorable wind on the northern Gulf of Mexico shelf, *Journal of Marine Systems*, *131*, 63-73, doi:https://doi.org/10.1016/j.jmarsys.2013.11.009.

Fuenzalida, R., W. Schneider, J. Garcés-Vargas, L. Bravo, and C. Lange (2009), Vertical and horizontal extension of the oxygen minimum zone in the eastern South Pacific Ocean, *Deep Sea Research Part II: Topical Studies in Oceanography*, *56*(16), 992-1003.

Gibson, R., and R. Atkinson (2003), Oxygen minimum zone benthos: adaptation and community response to hypoxia, *Oceanogr. Marine Biol. Annu. Rev*, *41*, 1-45.

Gilly, W. F., J. M. Beman, S. Y. Litvin, and B. H. Robison (2013), Oceanographic and Biological Effects of Shoaling of the Oxygen Minimum Zone, *Annual Review of Marine Science*, *5*(1), 393-420, doi:10.1146/annurev-marine-120710-100849.

Inatomi, M., T. Hajima, and A. Ito (2019), Fraction of nitrous oxide production in nitrification and its effect on total soil emission: A meta-analysis and global-scale sensitivity analysis using a process-based model, *PLOS ONE*, *14*(7), e0219159, doi:10.1371/journal.pone.0219159.

IPCC (2007), Climate Change 2007: Synthesis Report. Contribution of Working Groups I, II and III to the Fourth Assessment Report of the Intergovernmental Panel on Climate Change [Core Writing Team, Pachauri, R.K and Reisinger, A. (eds.)]. IPCC, Geneva, Switzerland, 104 pp.

Ji, Q., A. R. Babbin, A. Jayakumar, S. Oleynik, and B. B. Ward (2015), Nitrous oxide production by nitrification and denitrification in the Eastern Tropical South Pacific oxygen minimum zone, *Geophysical Research Letters*, *42*(24), 10,755-710,764, doi:https://doi.org/10.1002/2015GL066853.

Knowles, R. (1982), Denitrification, *Microbiological Reviews*, *46*(1), 43-70, doi:doi:10.1128/mr.46.1.43-70.1982.

Knowles, R. (1996), Denitrification: microbiology and ecology, *Life Support Biosph Sci*, *3*(1-2), 31-34.

Machida, T., T. Nakazawa, Y. Fujii, S. Aoki, and O. Watanabe (1995), Increase in the atmospheric nitrous oxide concentration during the last 250 years, *Geophysical Research Letters*, *22*(21), 2921-2924, doi:https://doi.org/10.1029/95GL02822.

Martens, D. A. (2005), DENITRIFICATION, in *Encyclopedia of Soils in the Environment*, edited by D. Hillel, pp. 378-382, Elsevier, Oxford, doi:https://doi.org/10.1016/B0-12-348530-4/00138-7.

Mullins, H. T., J. B. Thompson, K. McDougall, and T. L. Vercoutere (1985), Oxygen-minimum zone edge effects: evidence from the central California coastal upwelling system, *Geology*, *13*(7), 491-494.

Nevison, C. D., T. J. Lueker, and R. F. Weiss (2004), Quantifying the nitrous oxide source from coastal upwelling, *Global Biogeochemical Cycles*, *18*(1), doi:https://doi.org/10.1029/2003GB002110.

Oey, L.-Y., T. Ezer, and H.-C. Lee (2005), Loop Current, Rings and Related Circulation in the Gulf of Mexico: A Review of Numerical Models and Future Challenges, *Geophys. Monograph Ser.*, *161*, 31-56, doi:10.1029/161GM04.

Paulmier, A., D. Ruiz-Pino, and V. Garçon (2011), CO 2 maximum in the oxygen minimum zone (OMZ), *Biogeosciences*, *8*(2), 239-252.

Paulmier, A., D. Ruiz-Pino, V. Garçon, and L. Farías (2006), Maintaining of the Eastern South Pacific Oxygen Minimum Zone (OMZ) off Chile, *Geophysical Research Letters*, *33*(20), doi:https://doi.org/10.1029/2006GL026801.

Portmann, R. W., J. S. Daniel, and A. R. Ravishankara (2012), Stratospheric ozone depletion due to nitrous oxide: influences of other gases, *Philosophical Transactions of the Royal Society B: Biological Sciences*, *367*(1593), 1256-1264, doi:doi:10.1098/rstb.2011.0377.

Rabalais, N. N., R. E. Turner, and W. J. W. Jr. (2002), Gulf of Mexico Hypoxia, A.K.A. "The Dead Zone", *Annual Review of Ecology and Systematics*, *33*(1), 235-263, doi:10.1146/annurev.ecolsys.33.010802.150513.

Reichart, G.-J., L. Lourens, and W. Zachariasse (1998), Temporal variability in the northern Arabian Sea oxygen minimum zone (OMZ) during the last 225,000 years, *Paleoceanography*, *13*(6), 607-621.

Revell, L. E., F. Tummon, R. J. Salawitch, A. Stenke, and T. Peter (2015), The changing ozone depletion potential of N2O in a future climate, *Geophysical Research Letters*, *42*(22), 10,047-010,055, doi:https://doi.org/10.1002/2015GL065702.

Sarmiento, J. L. (2013), Chapter 3: Air-Sea Interface, in *Ocean Biogeochemical Dynamics*, edited, pp. 73-101, Princeton University Press, doi:doi:10.1515/9781400849079-004.

Syakila, A., and C. Kroeze (2011), The global nitrous oxide budget revisited, *Greenhouse Gas Measurement and Management*, *1*(1), 17-26, doi:10.3763/ghgmm.2010.0007.

Thamdrup, B., T. Dalsgaard, and N. P. Revsbech (2012), Widespread functional anoxia in the oxygen minimum zone of the Eastern South Pacific, *Deep Sea Research Part I: Oceanographic Research Papers*, *65*, 36-45, doi:https://doi.org/10.1016/j.dsr.2012.03.001.

Tian, H., et al. (2020), A comprehensive quantification of global nitrous oxide sources and sinks, *Nature*, *586*, 248-256, doi:10.1038/s41586-020-2780-0.

Walker, J. T., C. A. Stow, and C. Geron (2010), Nitrous Oxide Emissions from the Gulf of Mexico Hypoxic Zone, *Environmental Science & Technology*, *44*(5), 1617-1623, doi:10.1021/es902058t.

Walker, N., S. Myint, A. Babin, and A. Haag (2003), Advances in satellite radiometry for the surveillance of surface temperatures, ocean eddies and upwelling processes in the Gulf of Mexico using GOES-8 measurements during summer, *Geophysical Research Letters*, *30*(16), doi:https://doi.org/10.1029/2003GL017555.

Ward, B. B. (2013), Nitrification, edited, doi:10.1016/B978-0-12-409548-9.00697-7.

Ward, B. B., H. E. Glover, and F. Lipschultz (1989), Chemoautotrophic activity and nitrification in the oxygen minimum zone off Peru, *Deep Sea Research Part A. Oceanographic Research Papers*, *36*(7), 1031-1051, doi:https://doi.org/10.1016/0198-0149(89)90076-9.

Zamora, L. M., A. Oschlies, H. W. Bange, K. B. Huebert, J. D. Craig, A. Kock, and C. R. Löscher (2012), Nitrous oxide dynamics in low oxygen regions of the Pacific: insights from the MEMENTO database, *Biogeosciences*, *9*(12), 5007-5022, doi:10.5194/bg-9-5007-2012.

APPENDIX A: SCHADE 2019 AND 2021 FIGURES

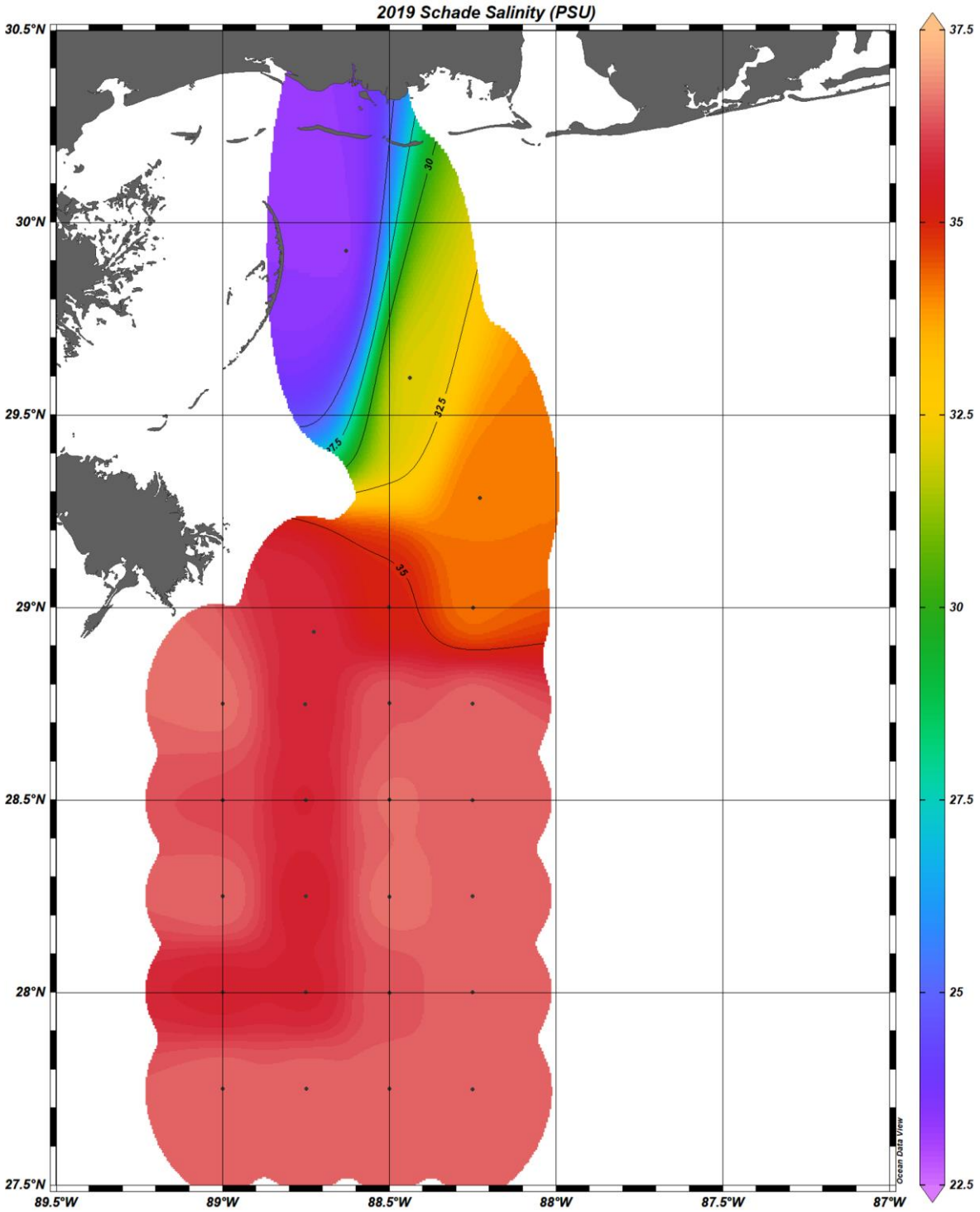

Figure A.1: Surface salinity (PSU) heat map for the Schade 2019 cruise area. The black dots indicate station locations.

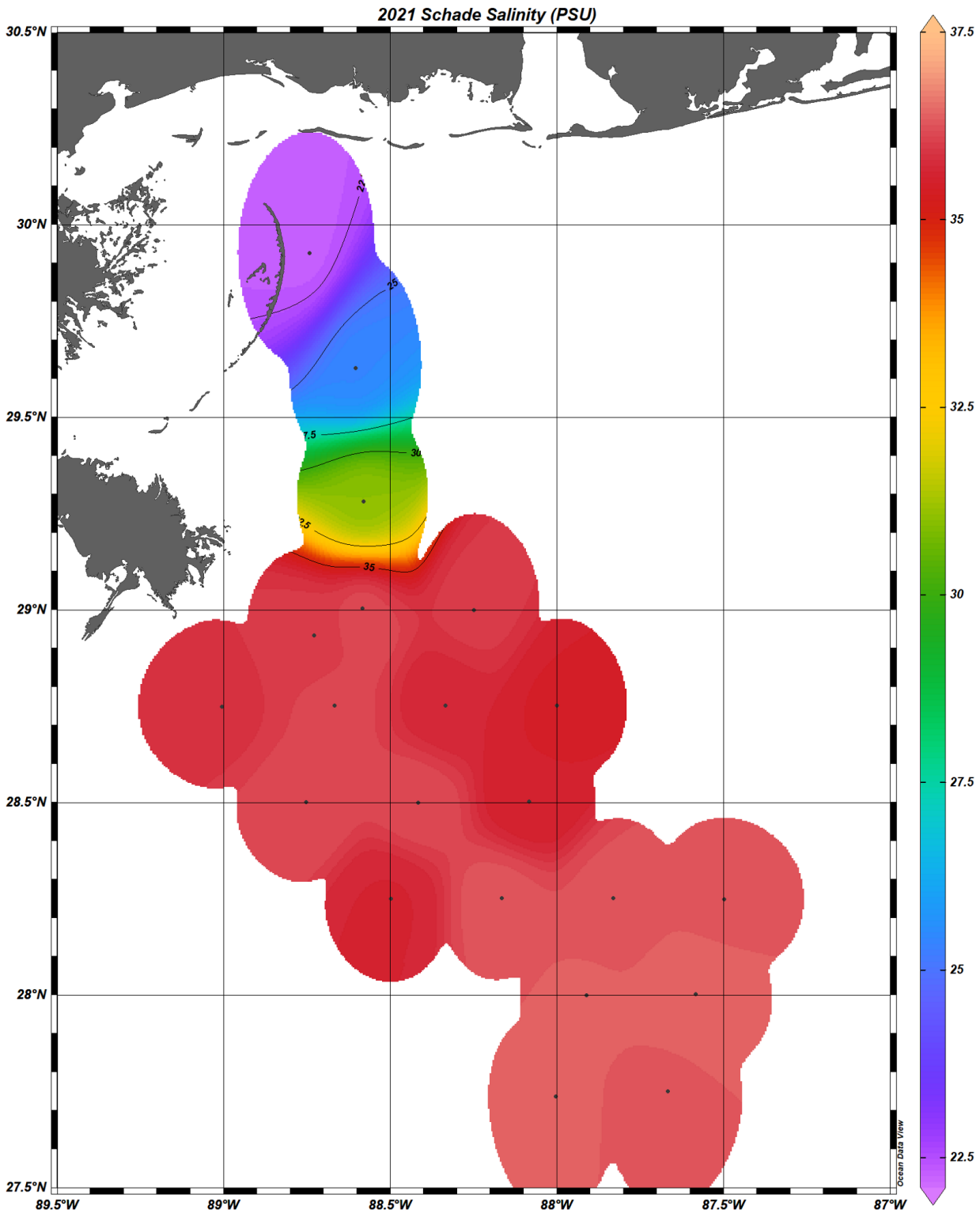

.

Figure A.2: Surface salinity (PSU) heat map for the Schade 2021 cruise area. The black dots indicate station locations.

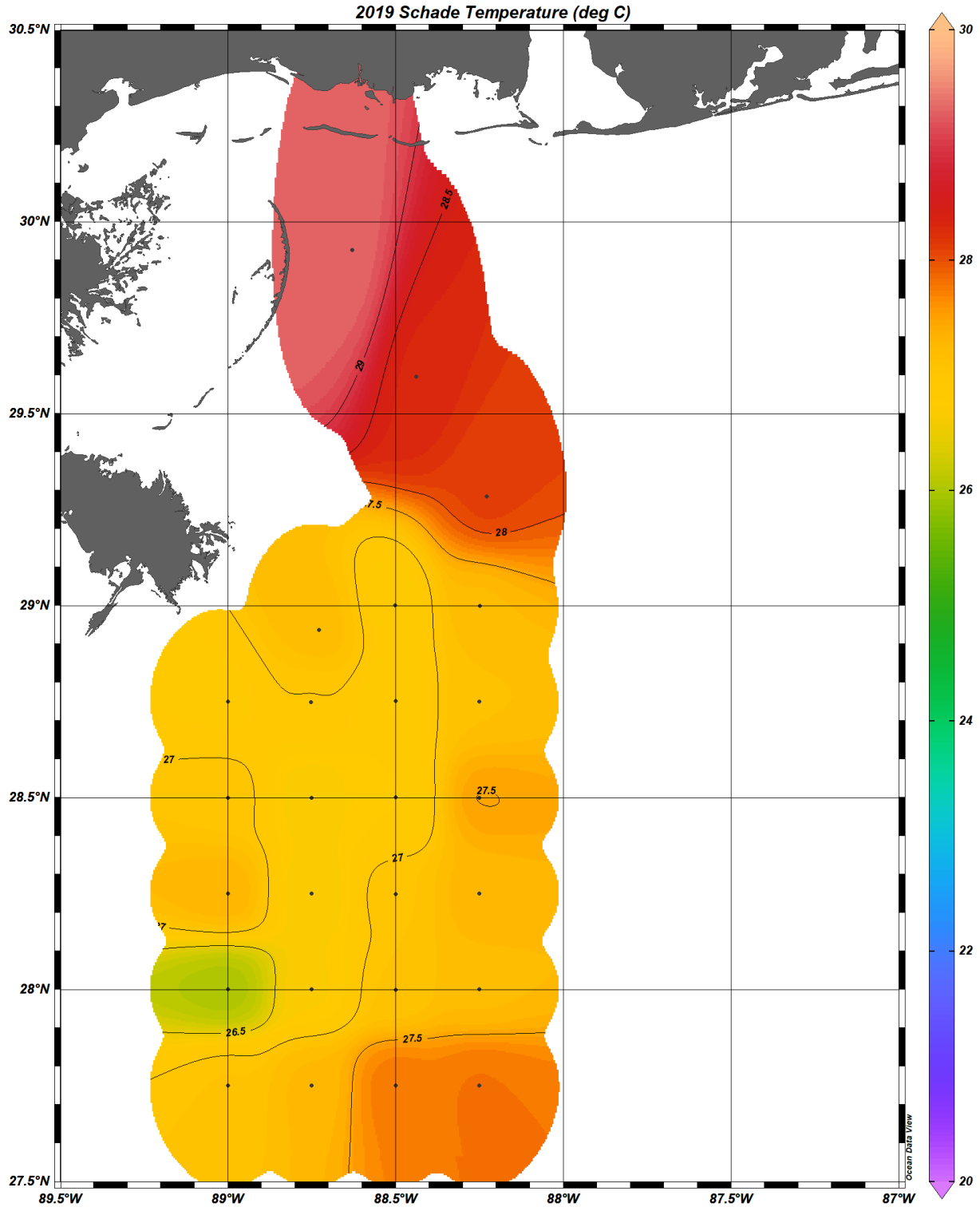

Figure A.3: Surface temperature (deg C) heat map for the Schade 2019 cruise area. The black dots indicate station locations.

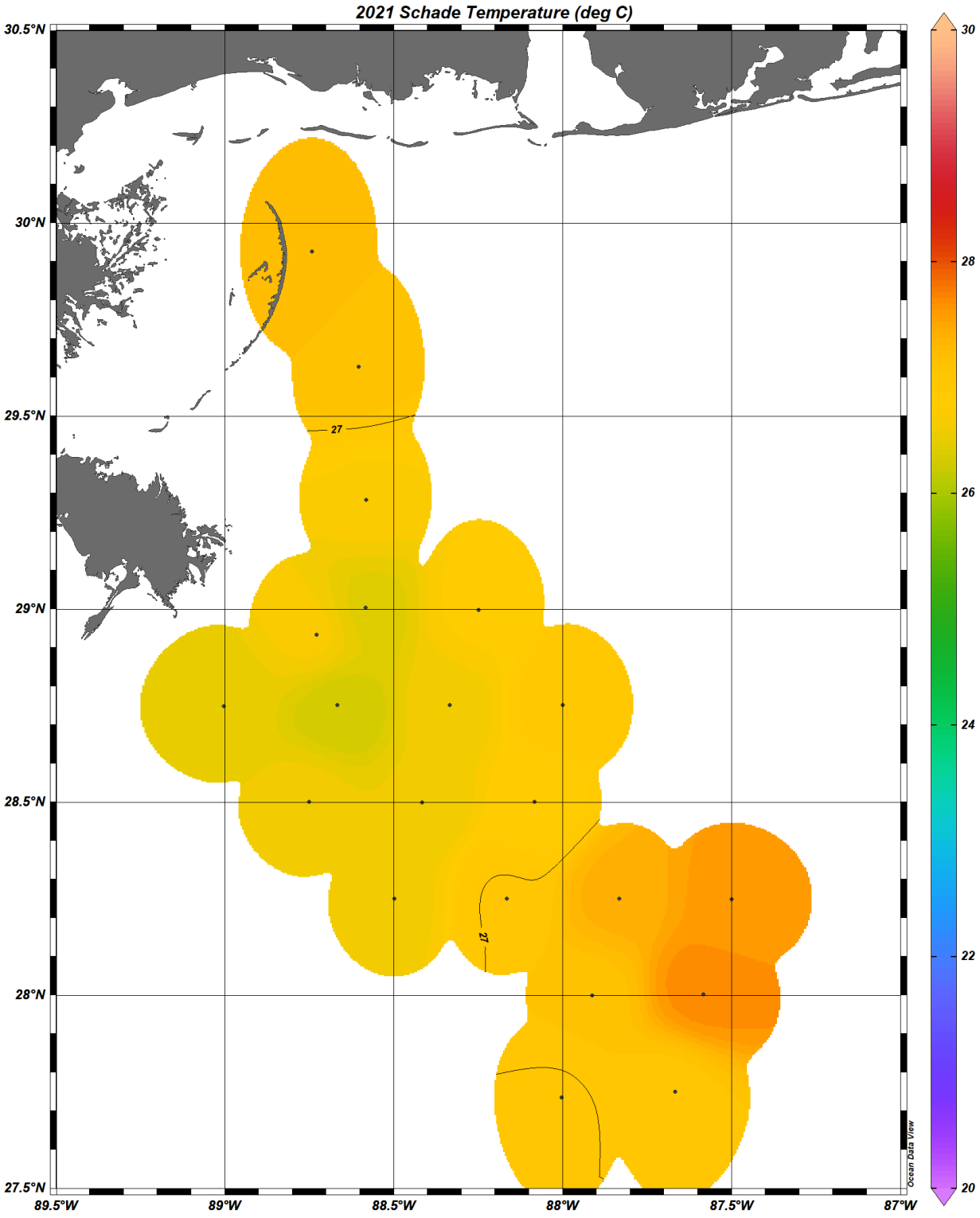

Figure A.4: Surface temperature (deg C) heat map for the Schade 2021 cruise area. The black dots indicate station locations.

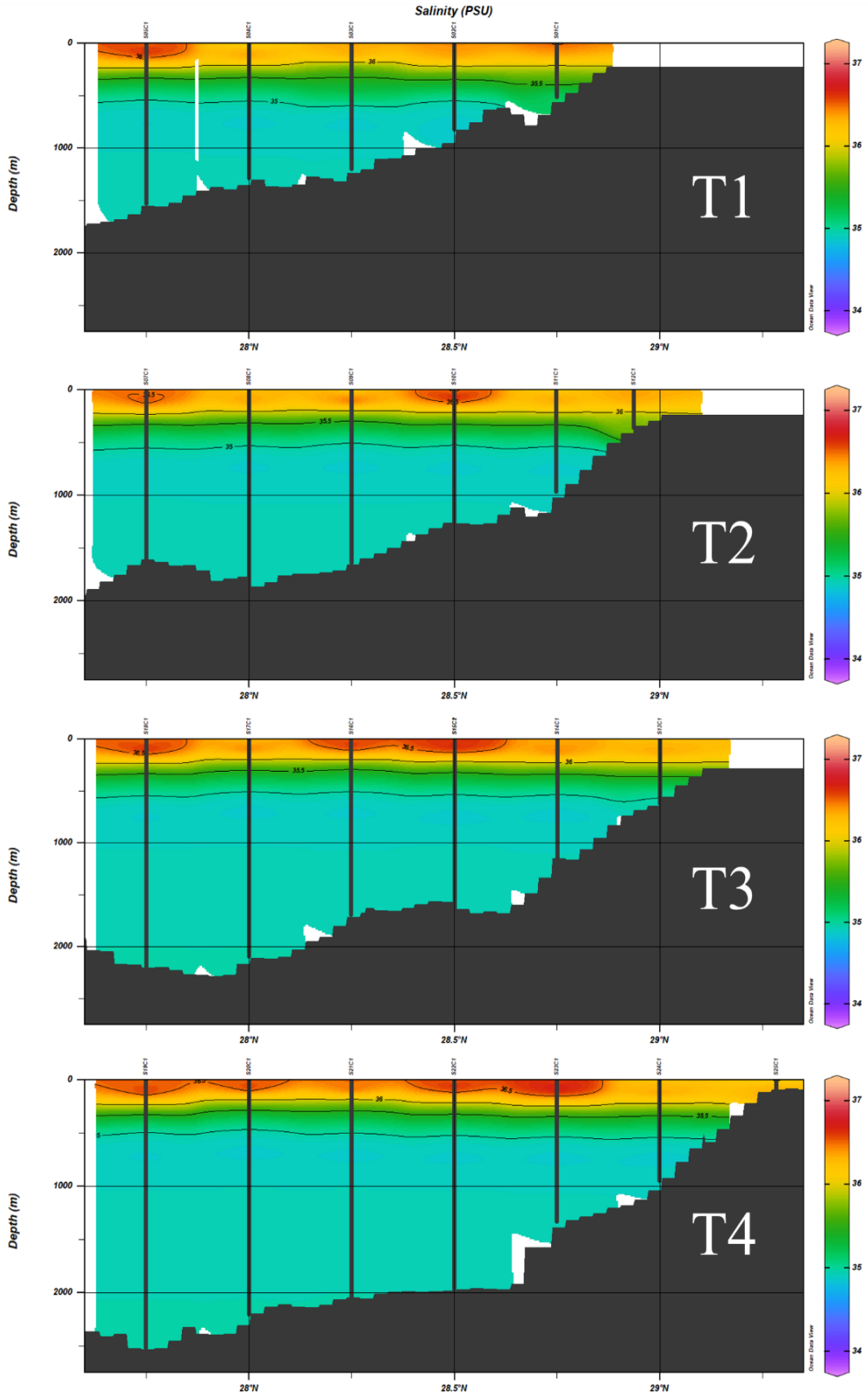

Figure A.5: Schade 2019 salinity (PSU) heat maps. Station labels are on the top axis of each plot and transect labels follow those in Figure 2.1. The black lines represent the location and depth of each data point.

.

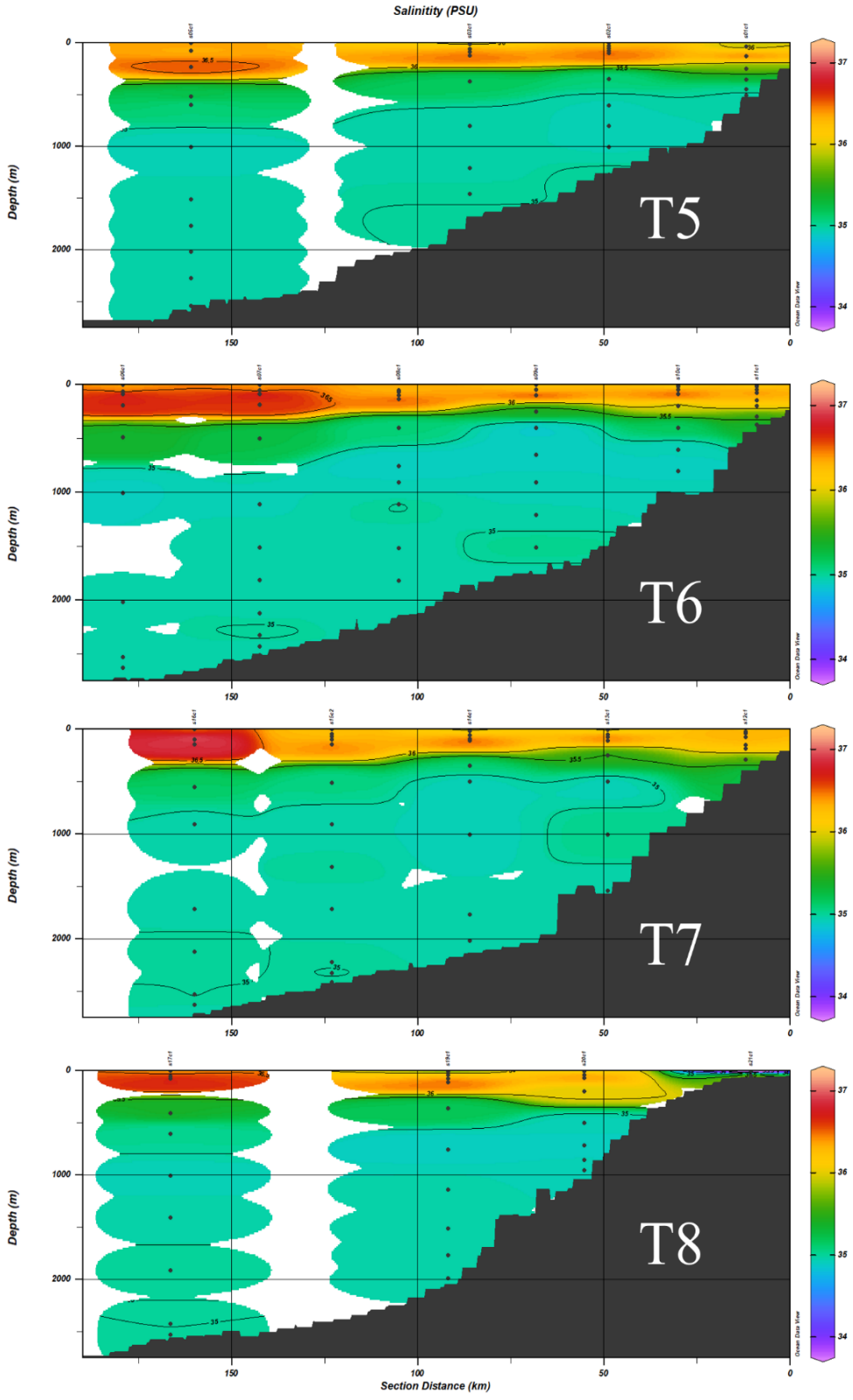

Figure A.6: Schade 2021 salinity (PSU) heat maps. Station labels are on the top axis of each plot and transect labels follow those in Figure 2.1. The black dots represent the location and depth of each data point.

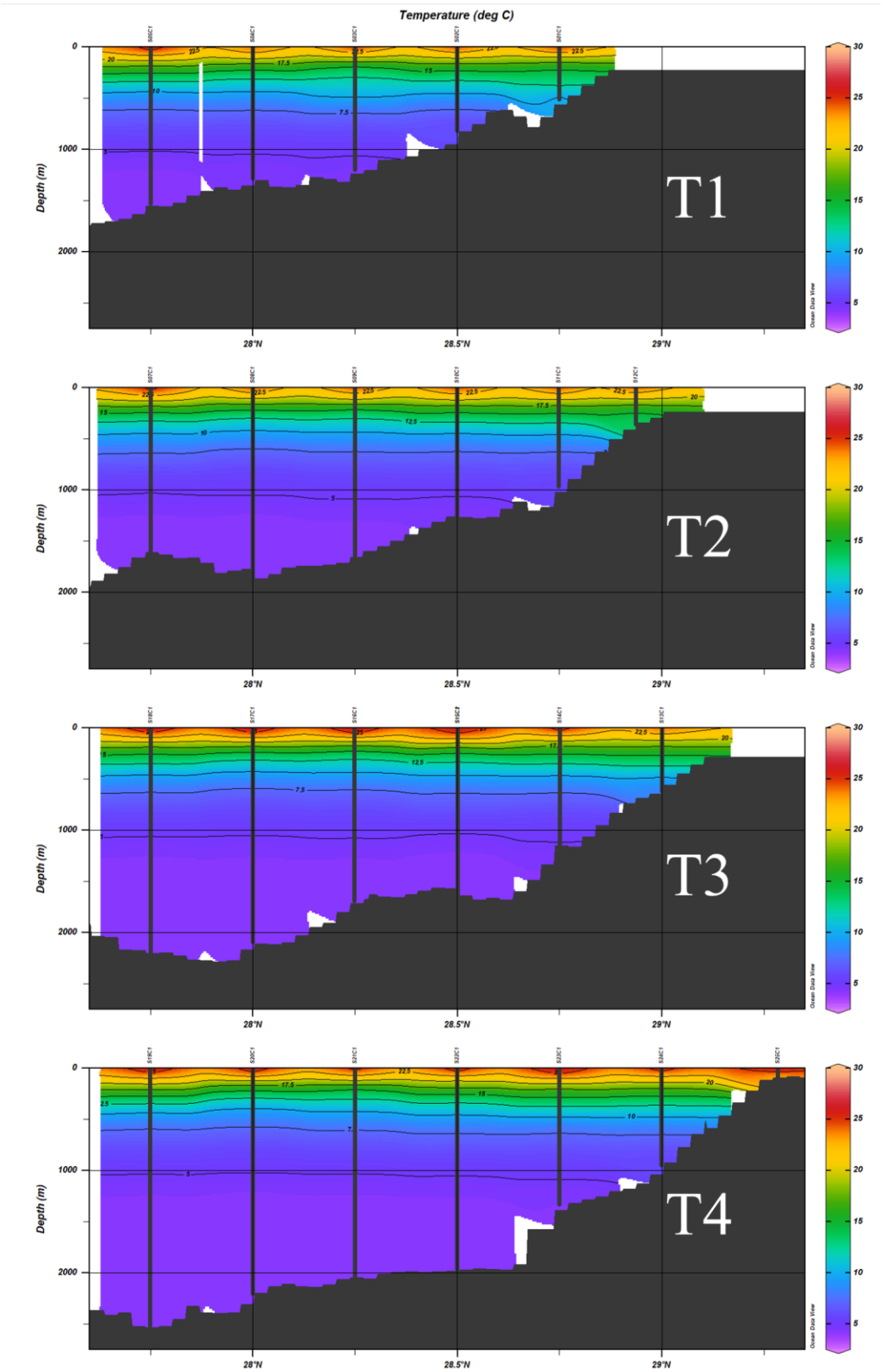

Figure A.7: Schade 2019 temperature (deg C) heat maps. Station labels are on the top axis of each plot and transect labels follow those in Figure 2.1. The black lines represent the location and depth of each data point.

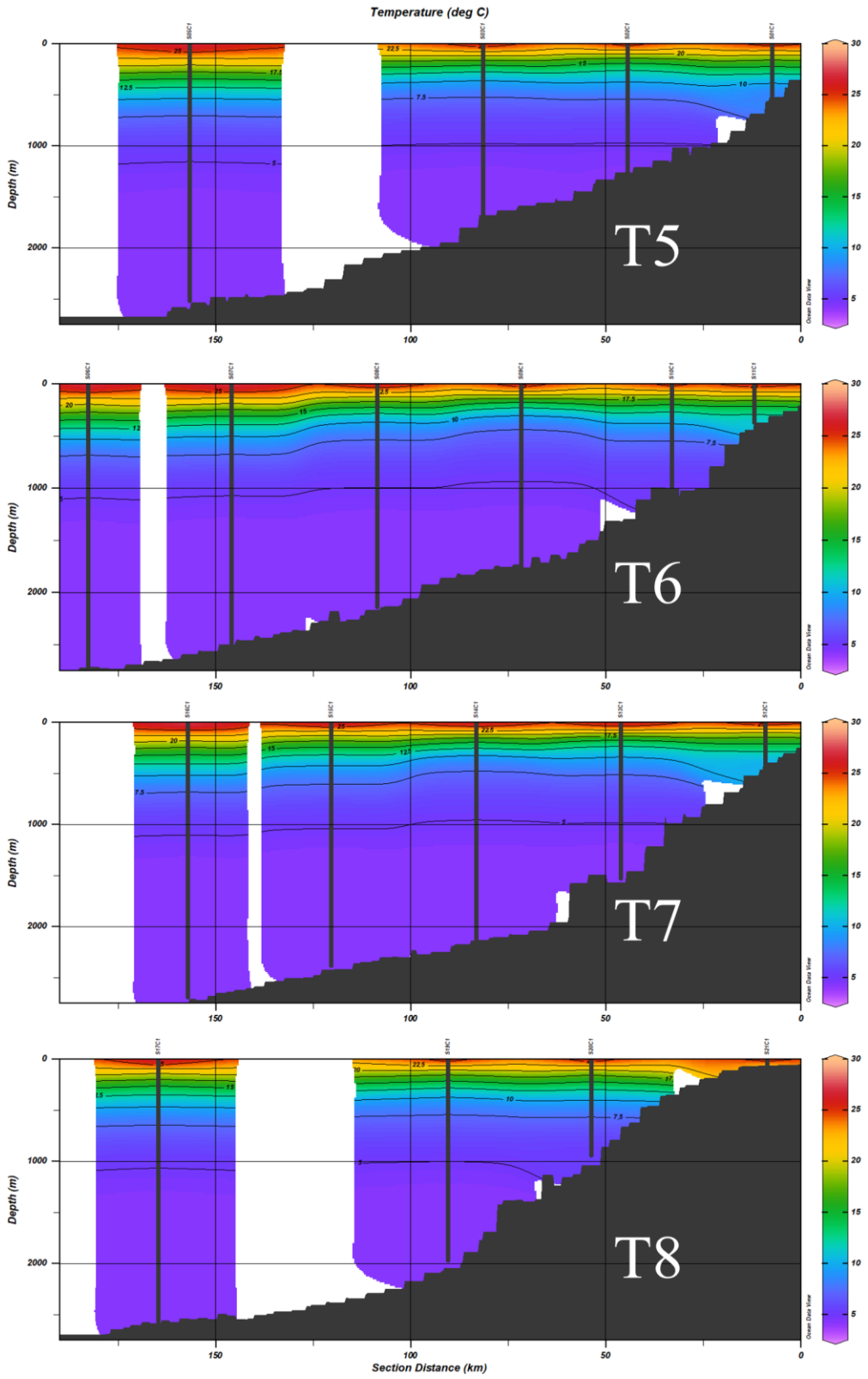

Figure A.8: Schade 2021 temperature (deg C) heat maps. Station labels are on the top axis of each plot and transect labels follow those in Figure 2.1. The black lines represent the location and depth of each data point.

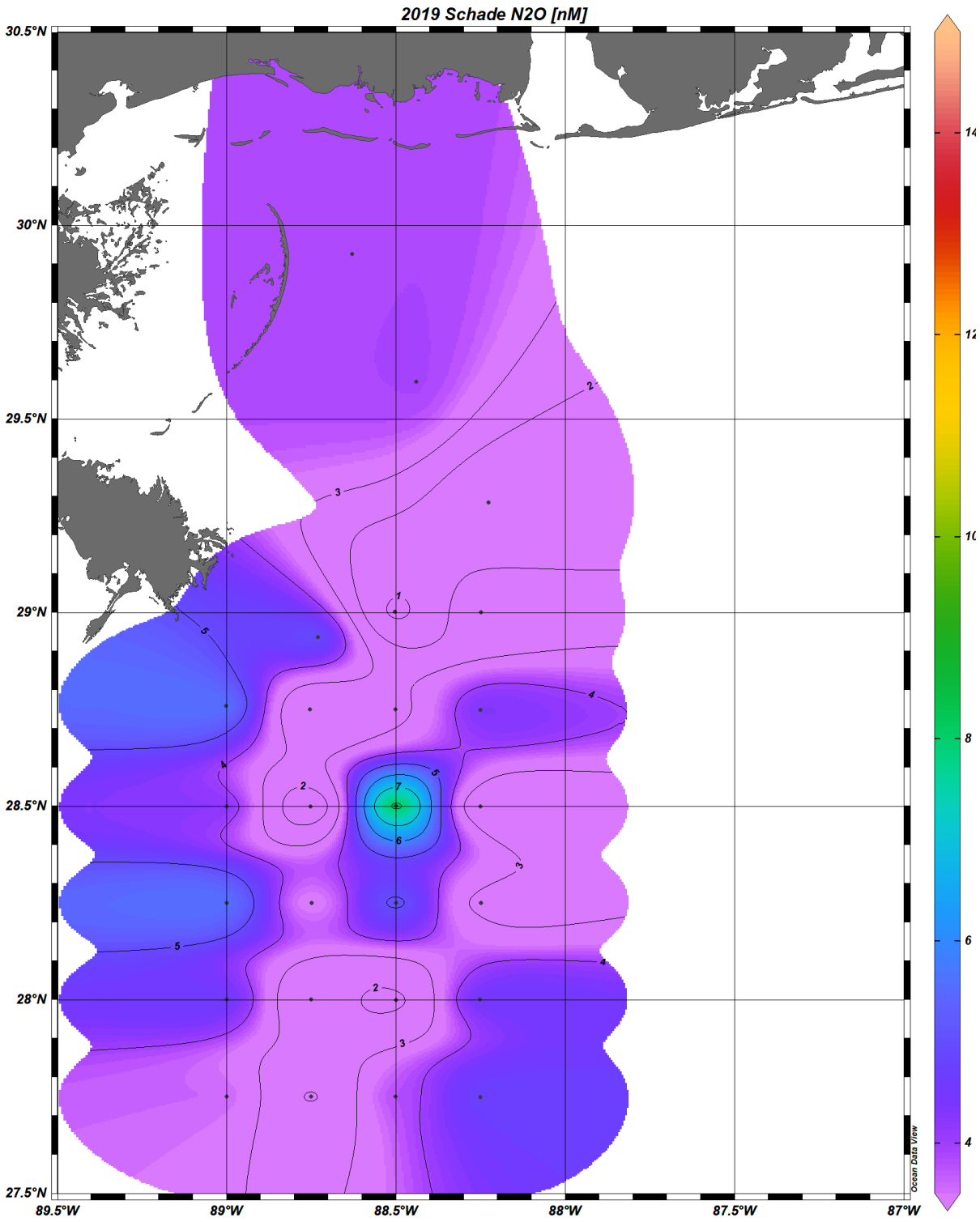

Figure A.9: Surface N_2O (nM) heat map for the Schade 2019 cruise area. The black dots indicate station locations.

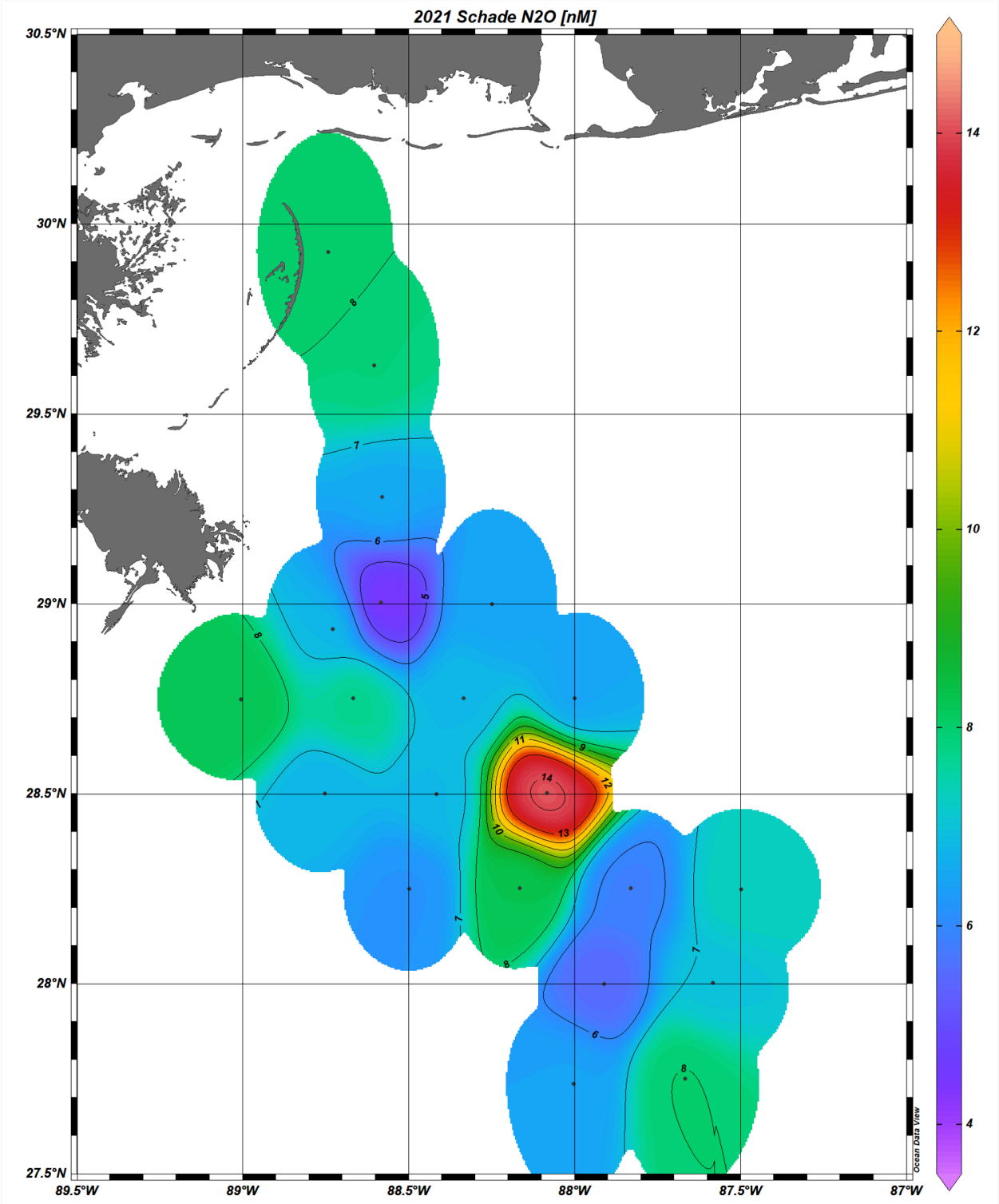

Figure A.10: Surface N_2O (nM) heat map for the Schade 2021 cruise area. The black dots indicate station locations.

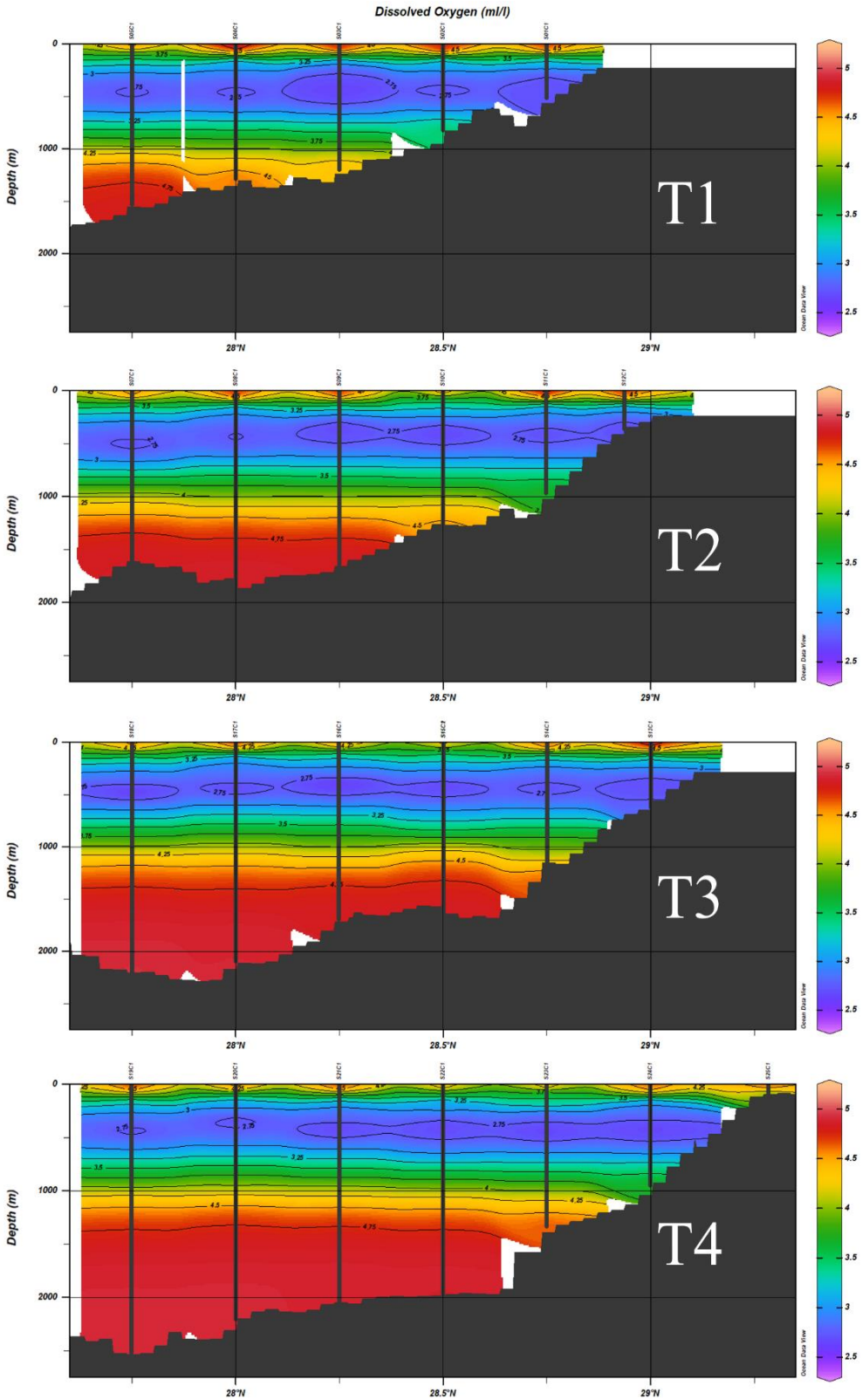

Figure A.11: Schade 2019 dissolved oxygen (ml/l) heat maps. Station labels are on the top axis of each plot and transect labels follow those in Figure 2.1. The black lines represent the location and depth of each data point.

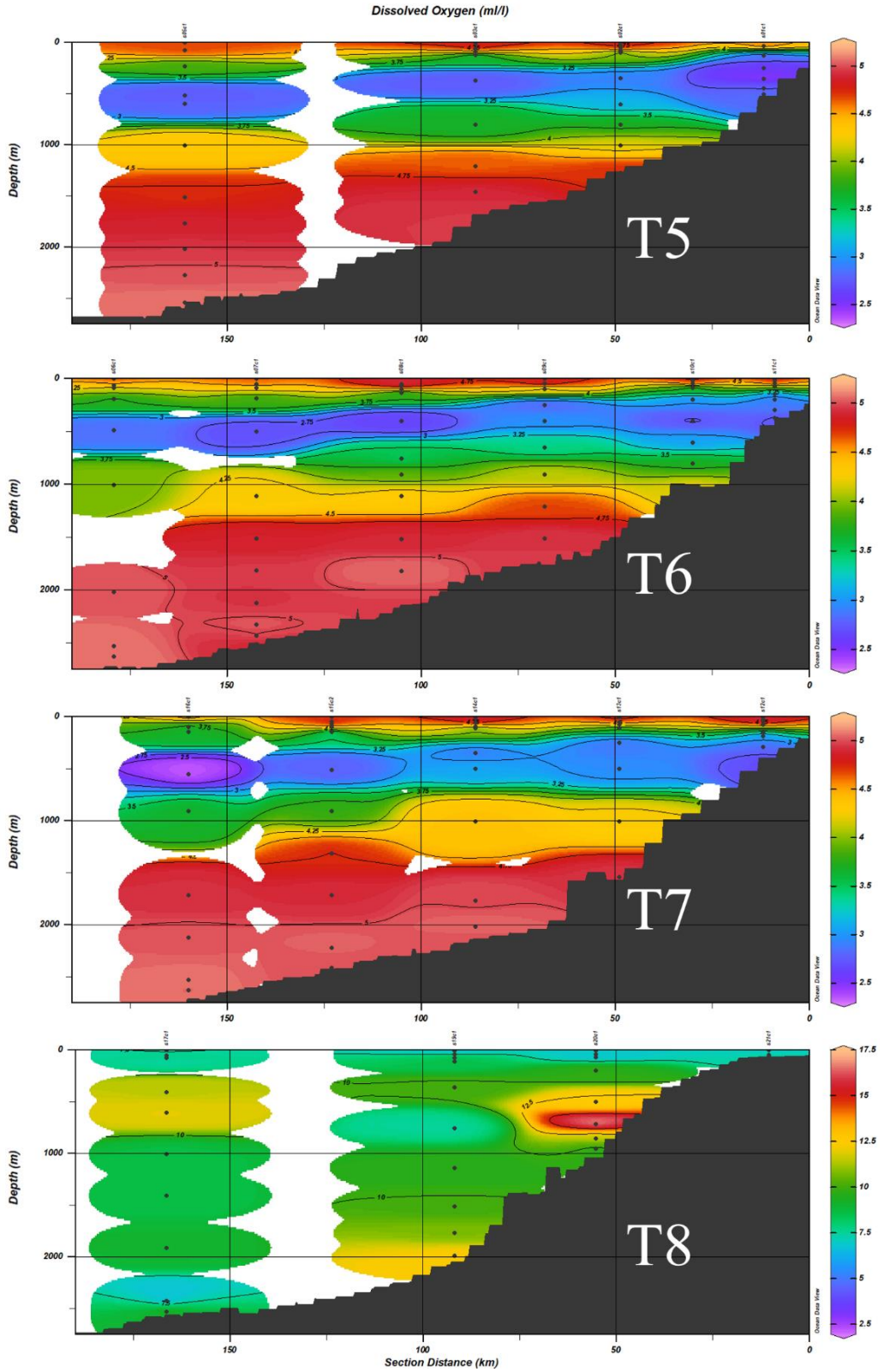

Figure A.12: Schade 2021 dissolved oxygen (ml/l) heat maps. Station labels are on the top axis of each plot and transect labels follow those in Figure 2.1. The black dots represent the location and depth of each data point.

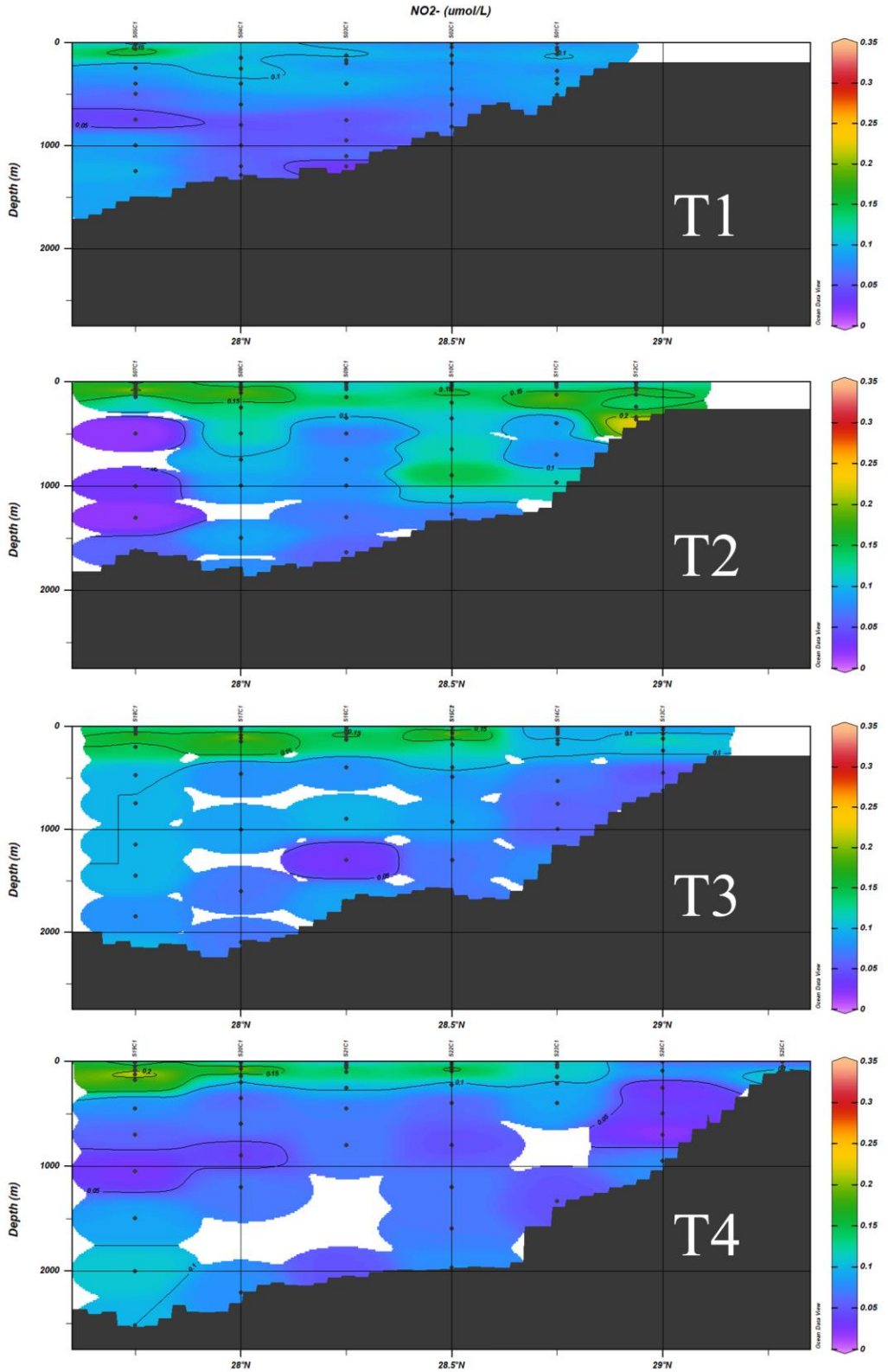

Figure A.13: Schade 2019 NO_3^- (µmol/L) heat maps. Station labels are on the top axis of each plot and transect labels follow those in Figure 2.1. The black dots represent the location and depth of each data point.

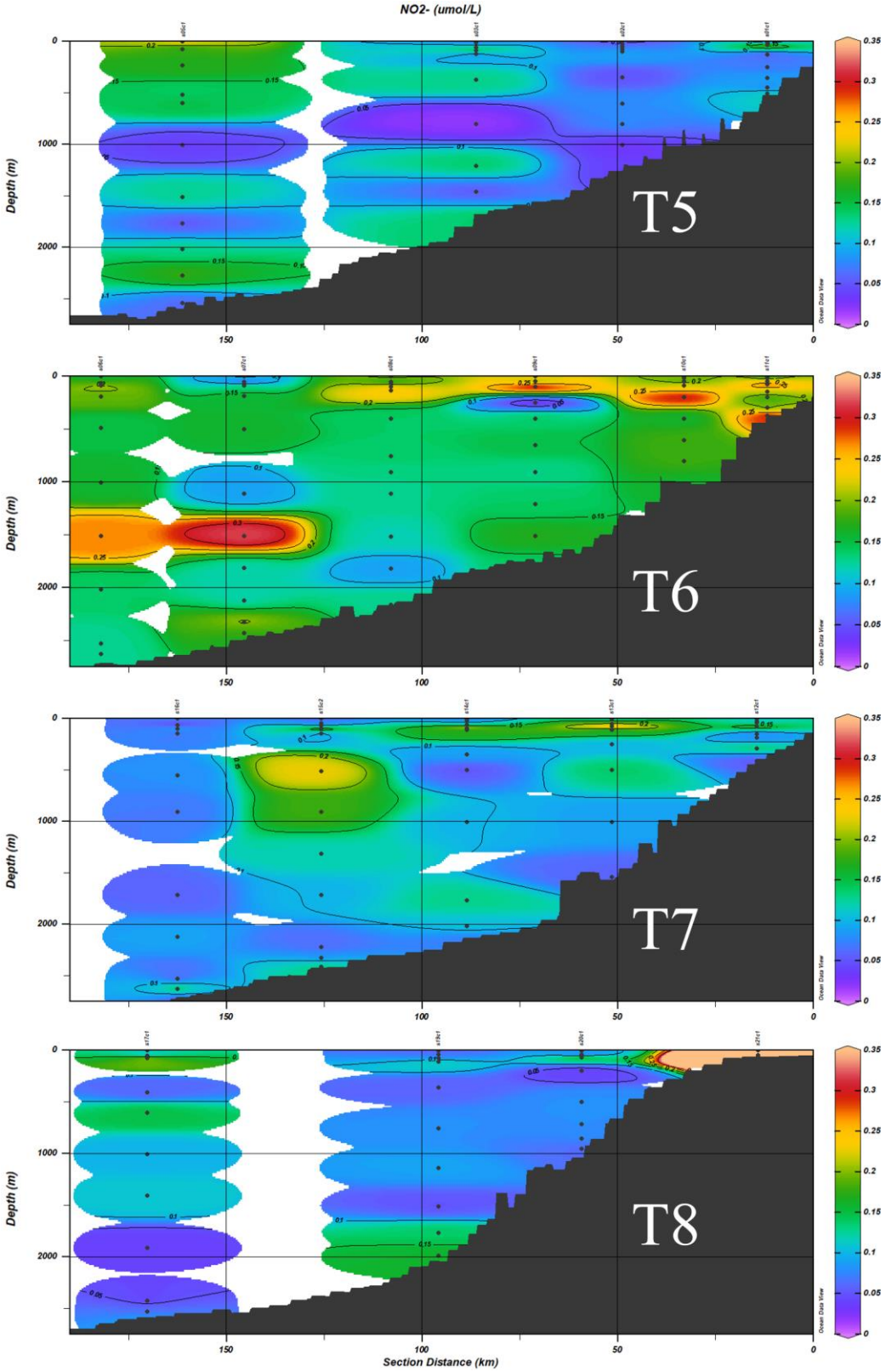

Figure A.14: Schade 2021 NO_3^- (µmol/L) heat maps. Station labels are on the top axis of each plot and transect labels follow those in Figure 2.1. The black dots represent the location and depth of each data point.

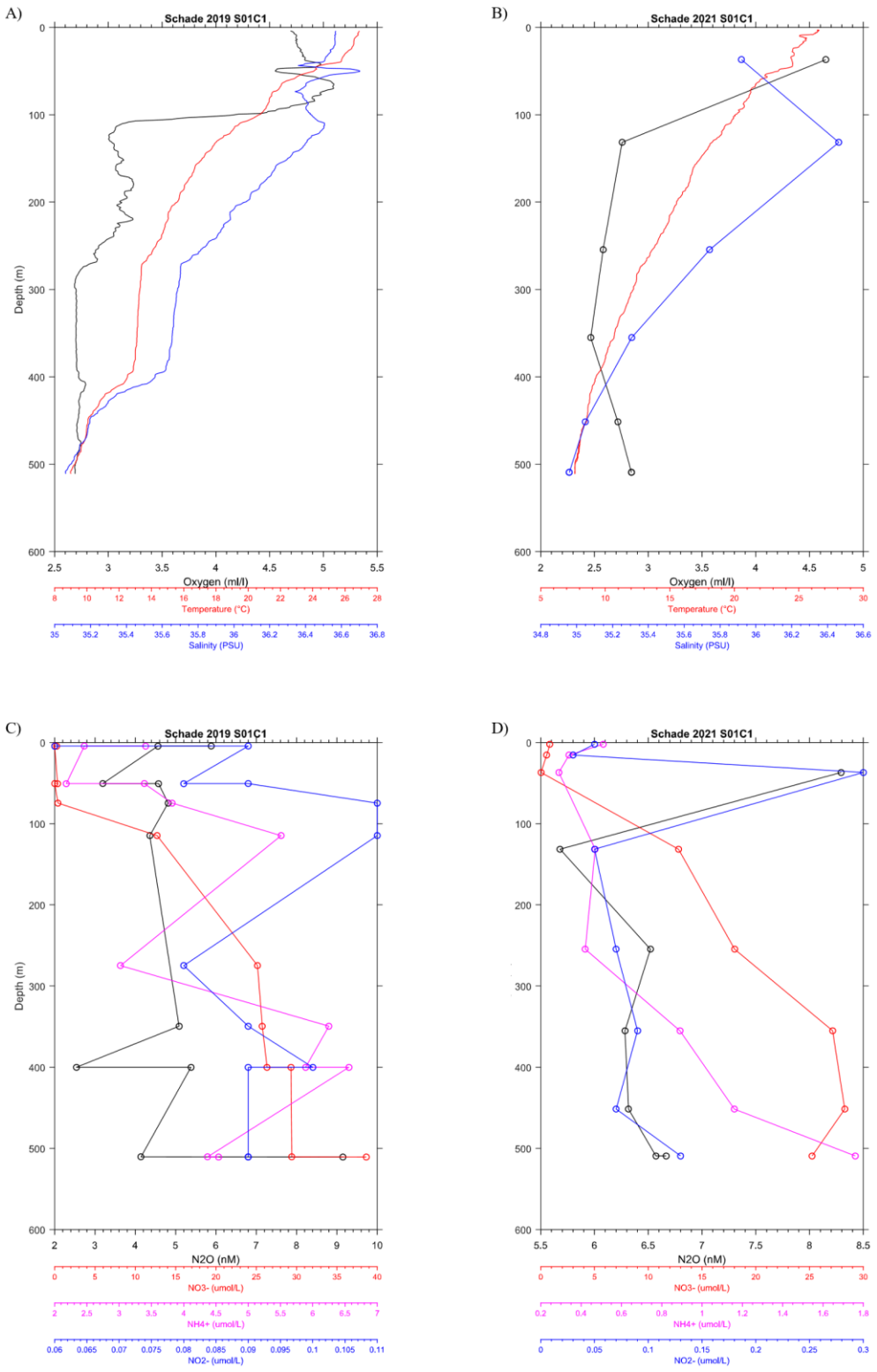

Figure A.15: Shared station vertical plots of physical properties (A and B) and nitrogen species (C and D) values between Schade 2019 and 2021 cruises for stations 1 and 1 respectively. Physical properties include temperature (deg C), salinity (PSU), and dissolved oxygen (ml/l). Nitrogen species include NO_3^-, NO_2^{--}, and NH_4^+all in units of µmol/L.

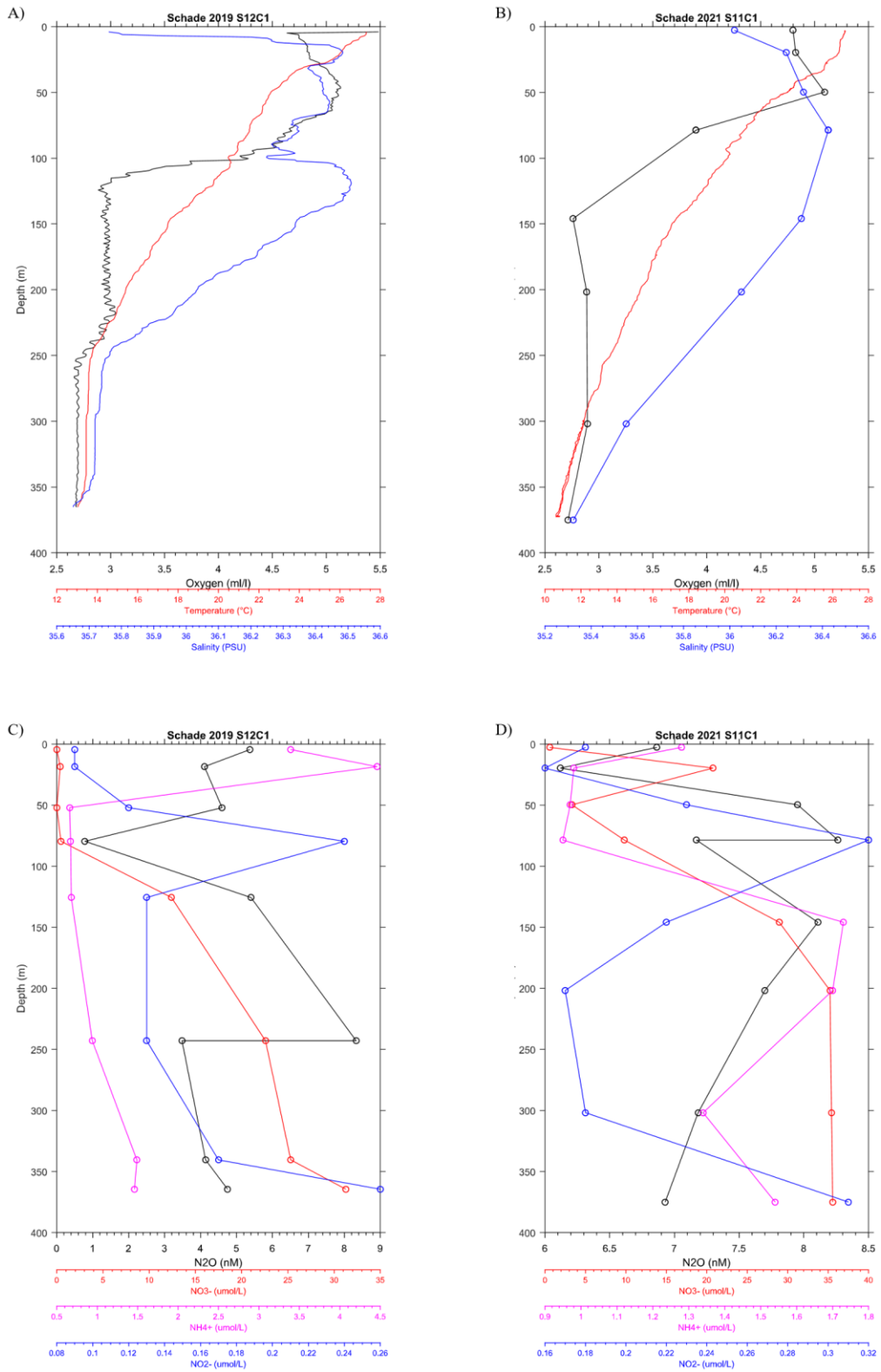

Figure A.16: Shared station vertical plots of physical properties (A and B) and nitrogen species (C and D) values between Schade 2019 and 2021 cruises for stations 12 and 11 respectively. Physical properties include temperature (deg C), salinity (PSU), and dissolved oxygen (ml/l). Nitrogen species include NO_3^-, NO_2^{--}, and NH_4^+ all in units of µmol/L.

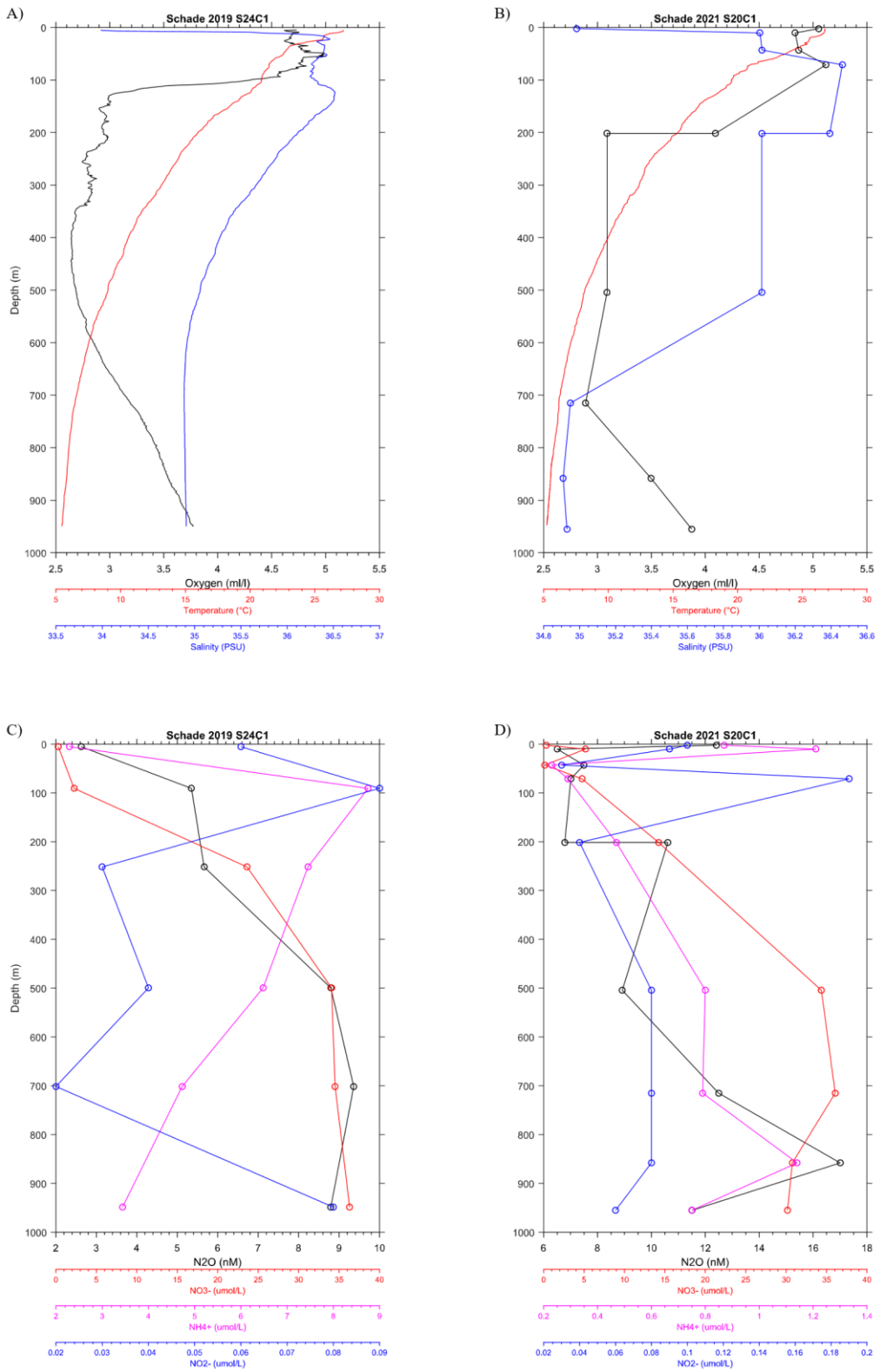

Figure A.17: Shared station vertical plots of physical properties (A and B) and nitrogen species (C and D) values between Schade 2019 and 2021 cruises for stations 24 and 20 respectively. Physical properties include temperature (deg C), salinity (PSU), and dissolved oxygen (ml/l). Nitrogen species include NO_3^-, NO_2^{--}, and NH_4^+ all in units of µmol/L.

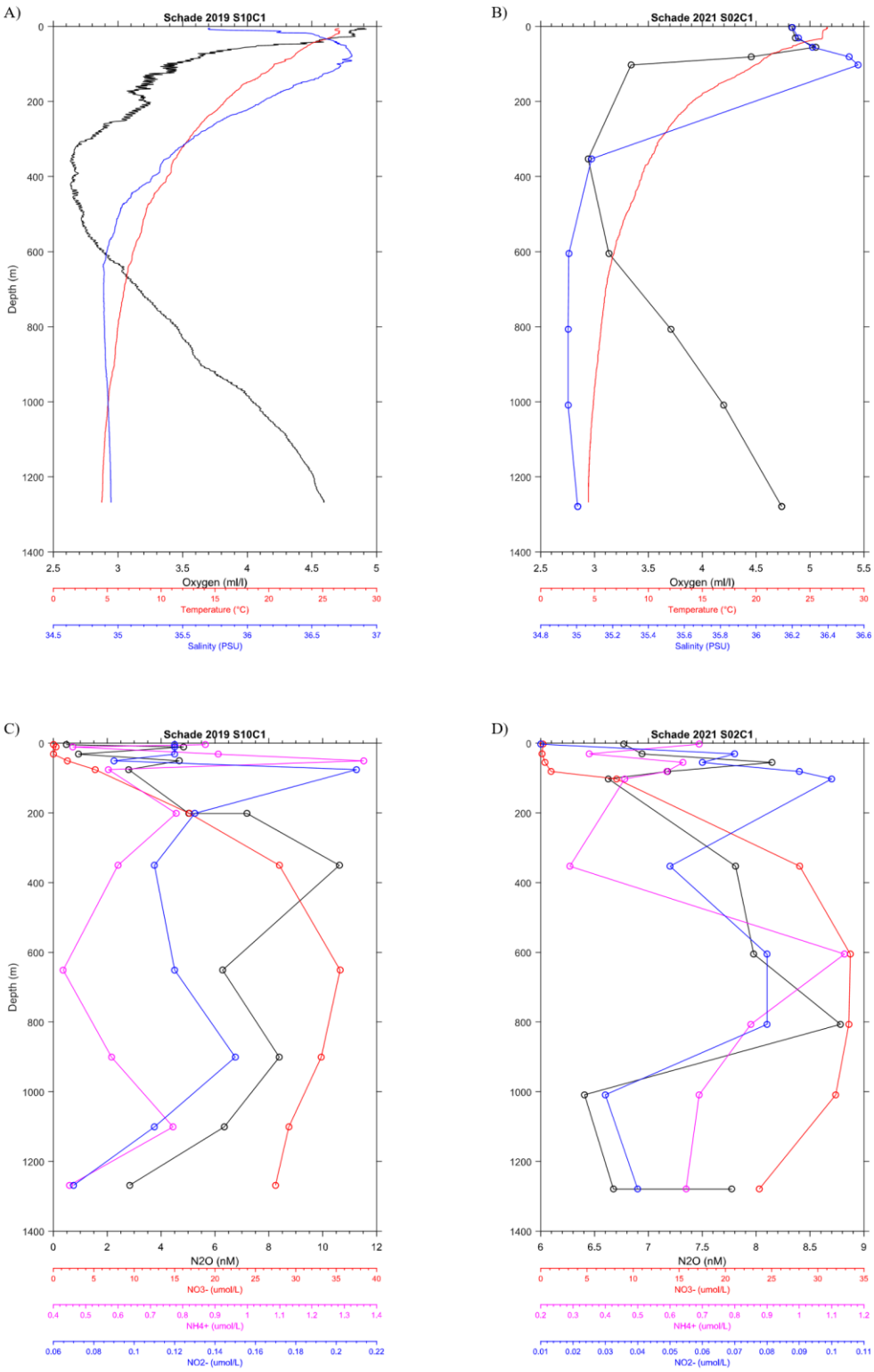

Figure A.18: Shared station vertical plots of physical properties (A and B) and nitrogen species (C and D) values between Schade 2019 and 2021 cruises for stations 10 and 2 respectively. Physical properties include temperature (deg C), salinity (PSU), and dissolved oxygen (ml/l). Nitrogen species include NO_3^-, NO_2^{--}, and NH_4^+ all in units of µmol/L.

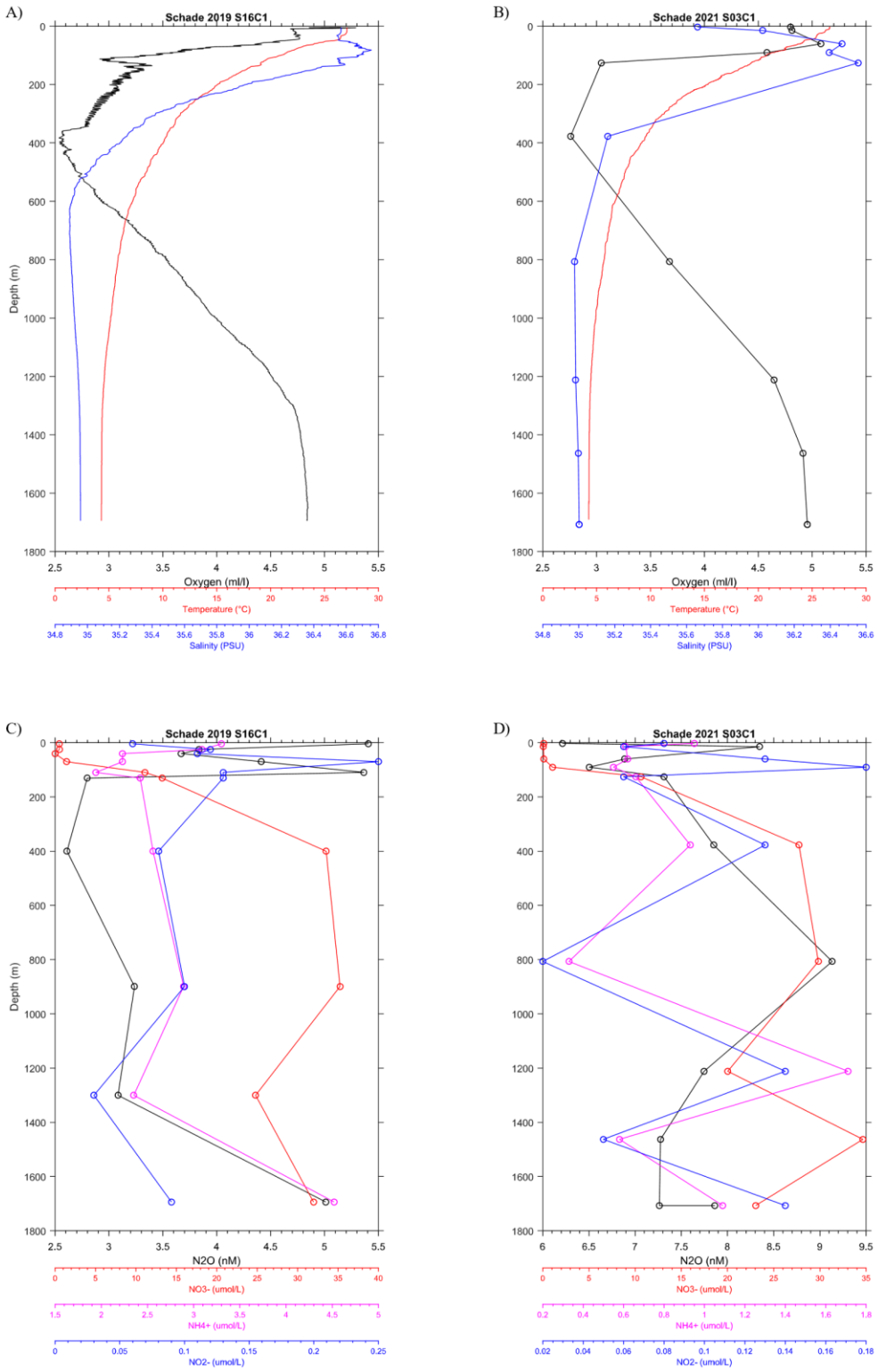

Figure A.19: Shared station vertical plots of physical properties (A and B) and nitrogen species (C and D) values between Schade 2019 and 2021 cruises for stations 16 and 3 respectively. Physical properties include temperature (deg C), salinity (PSU), and dissolved oxygen (ml/l). Nitrogen species include NO_3^-, NO_2^{--}, and NH_4^+ all in units of µmol/L.

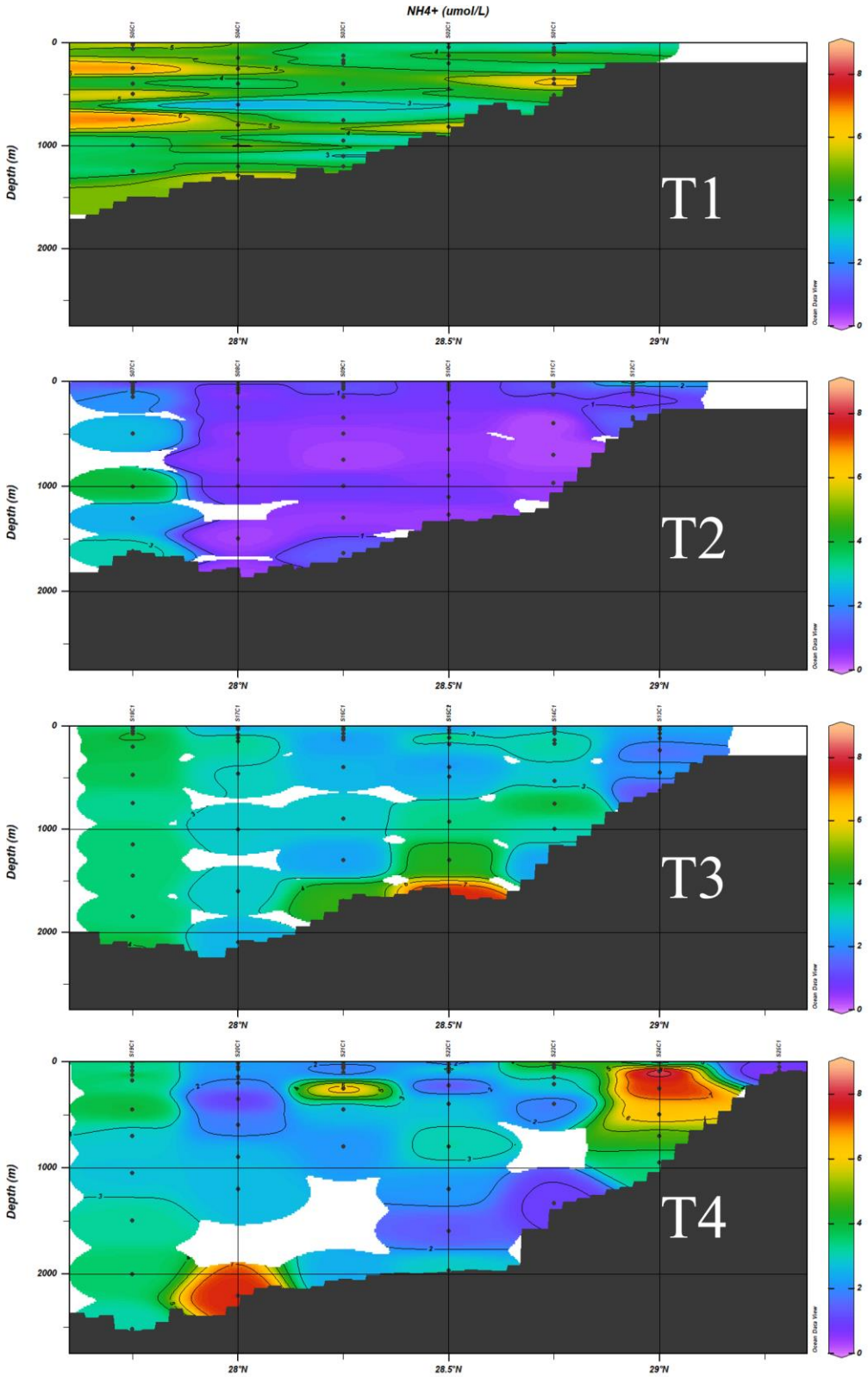

Figure A.20: Schade 2019 NH_4^+ (µmol/L) heat maps. Station labels are on the top axis of each plot and transect labels follow those in Figure 2.1. The black dots represent the location and depth of each data point.

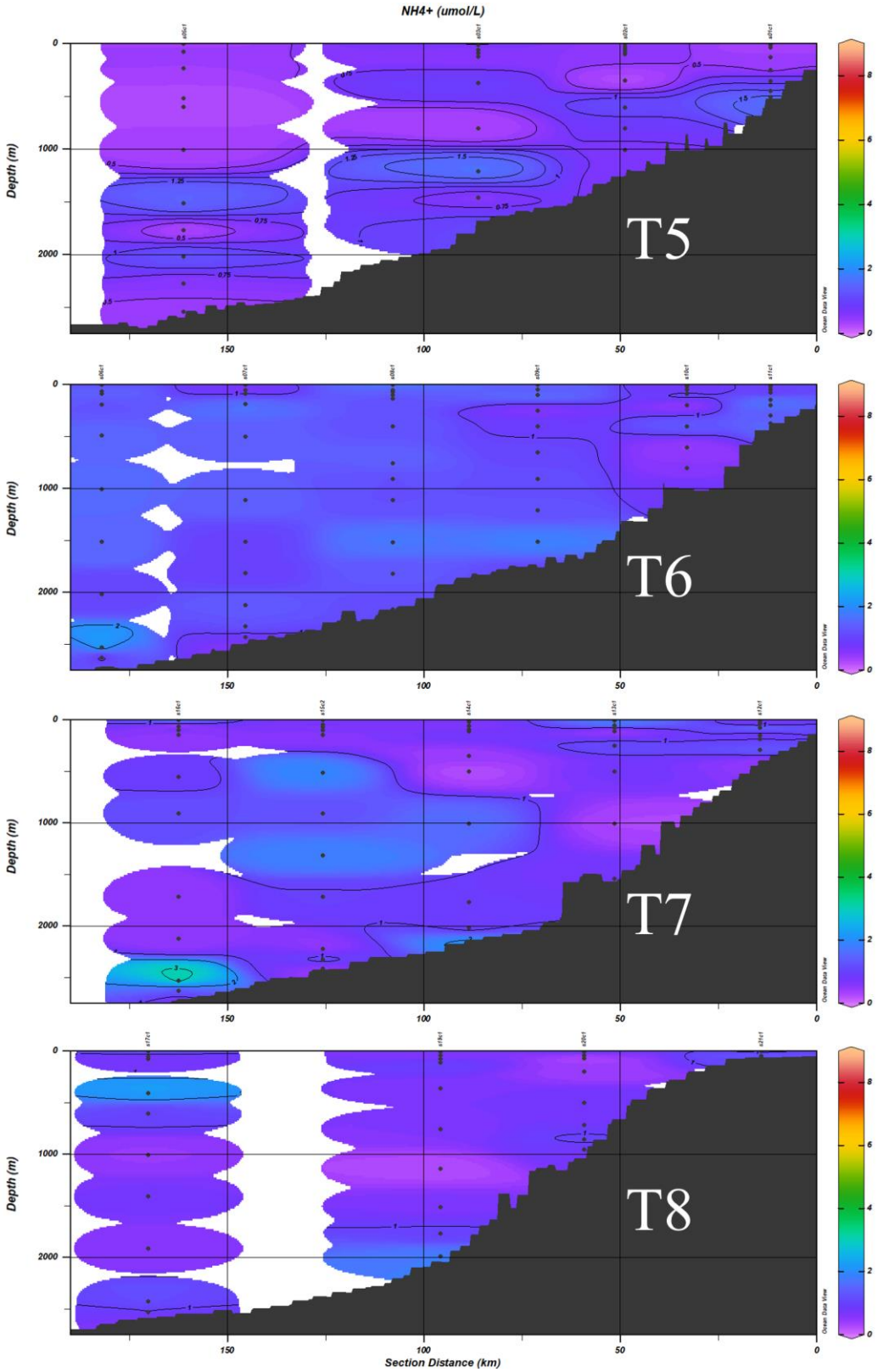

Figure A.21: Schade 2021 NH_4^+ (µmol/L) heat maps. Station labels are on the top axis of each plot and transect labels follow those in Figure 2.1. The black dots represent the location and depth of each data point.

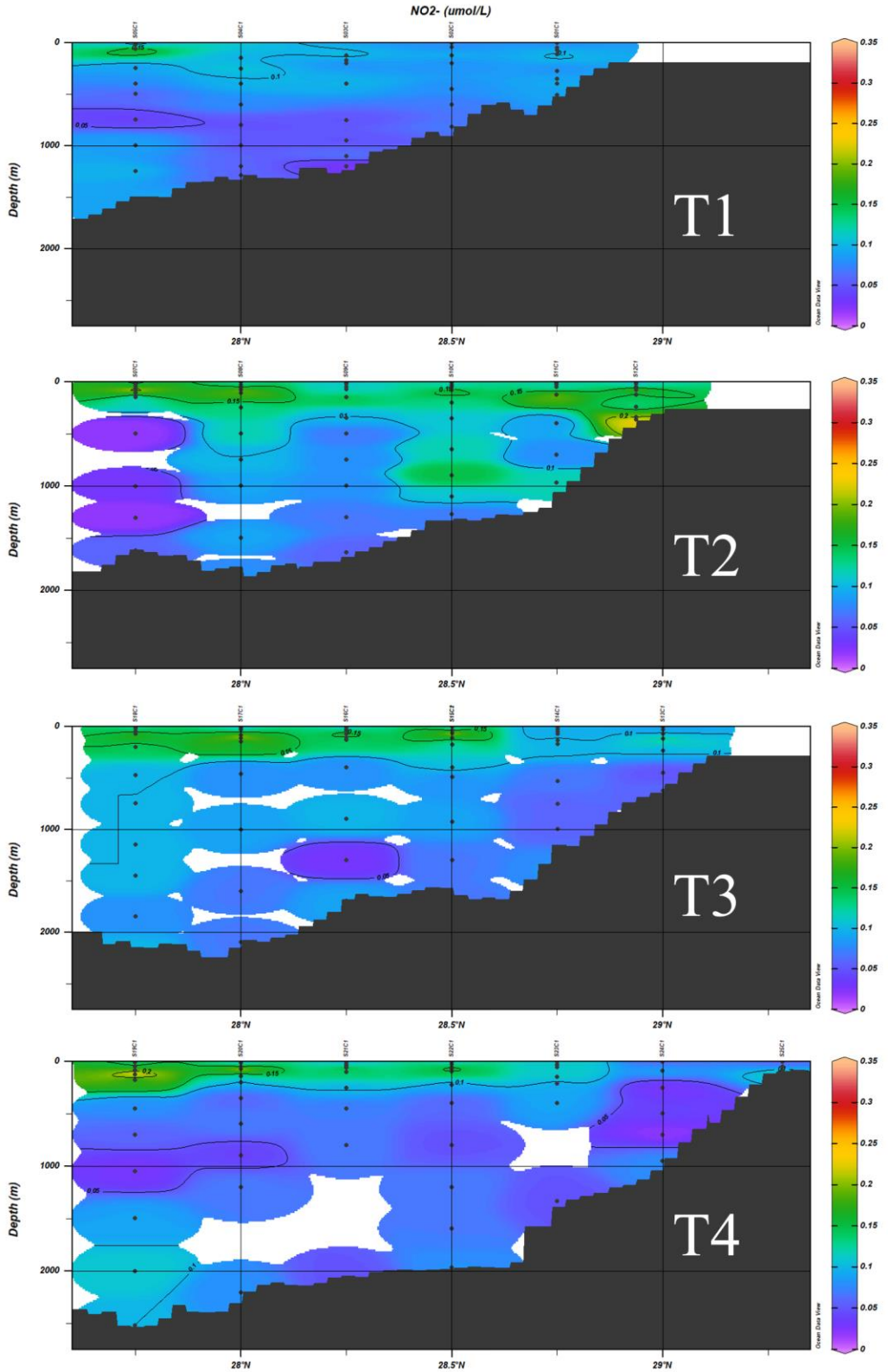

Figure A.22: Schade 2019 NO_2^- (µmol/L) heat maps. Station labels are on the top axis of each plot and transect labels follow those in Figure 2.1. The black dots represent the location and depth of each data point.

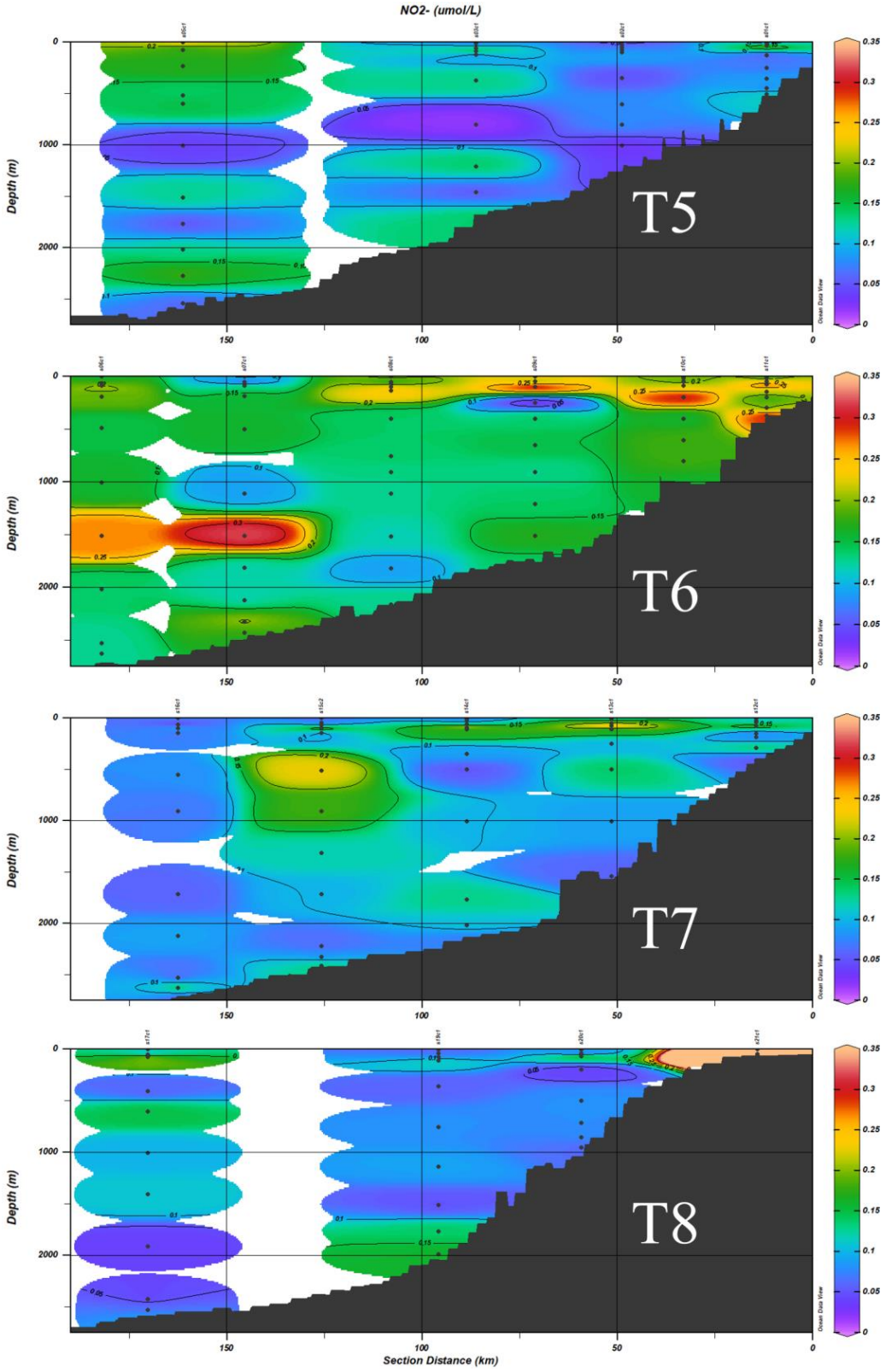

Figure A.23: Schade 2021 NO_2^- (µmol/L) heat maps. Station labels are on the top axis of each plot and transect labels follow those in Figure 2.1. The black dots represent the location and depth of each data point.

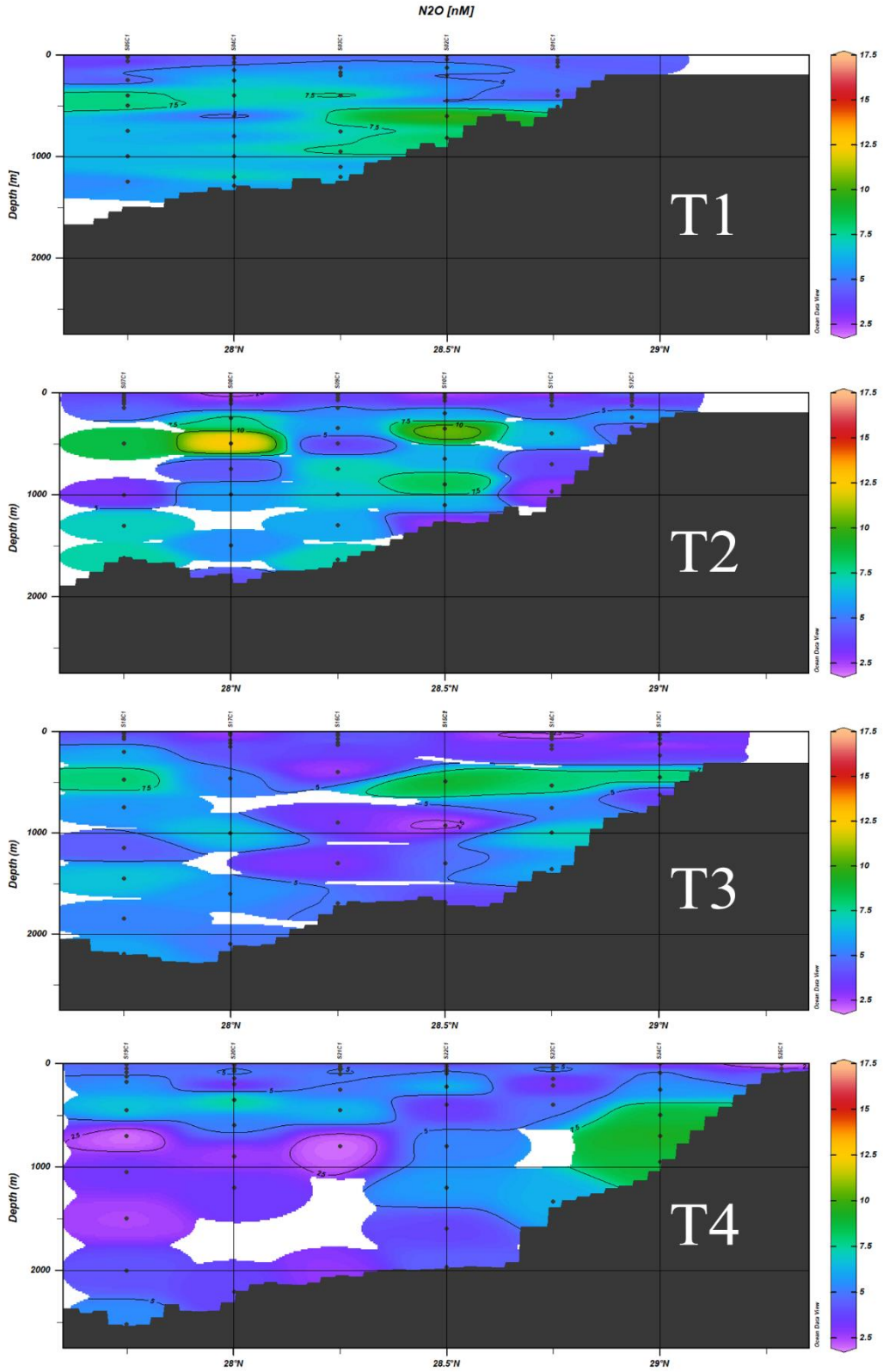

Figure A.24: Schade 2019 N_2O (nM) heat maps. Station labels are on the top axis of each plot and transect labels follow those in Figure 2.1. The black dots represent the location and depth of each data point.

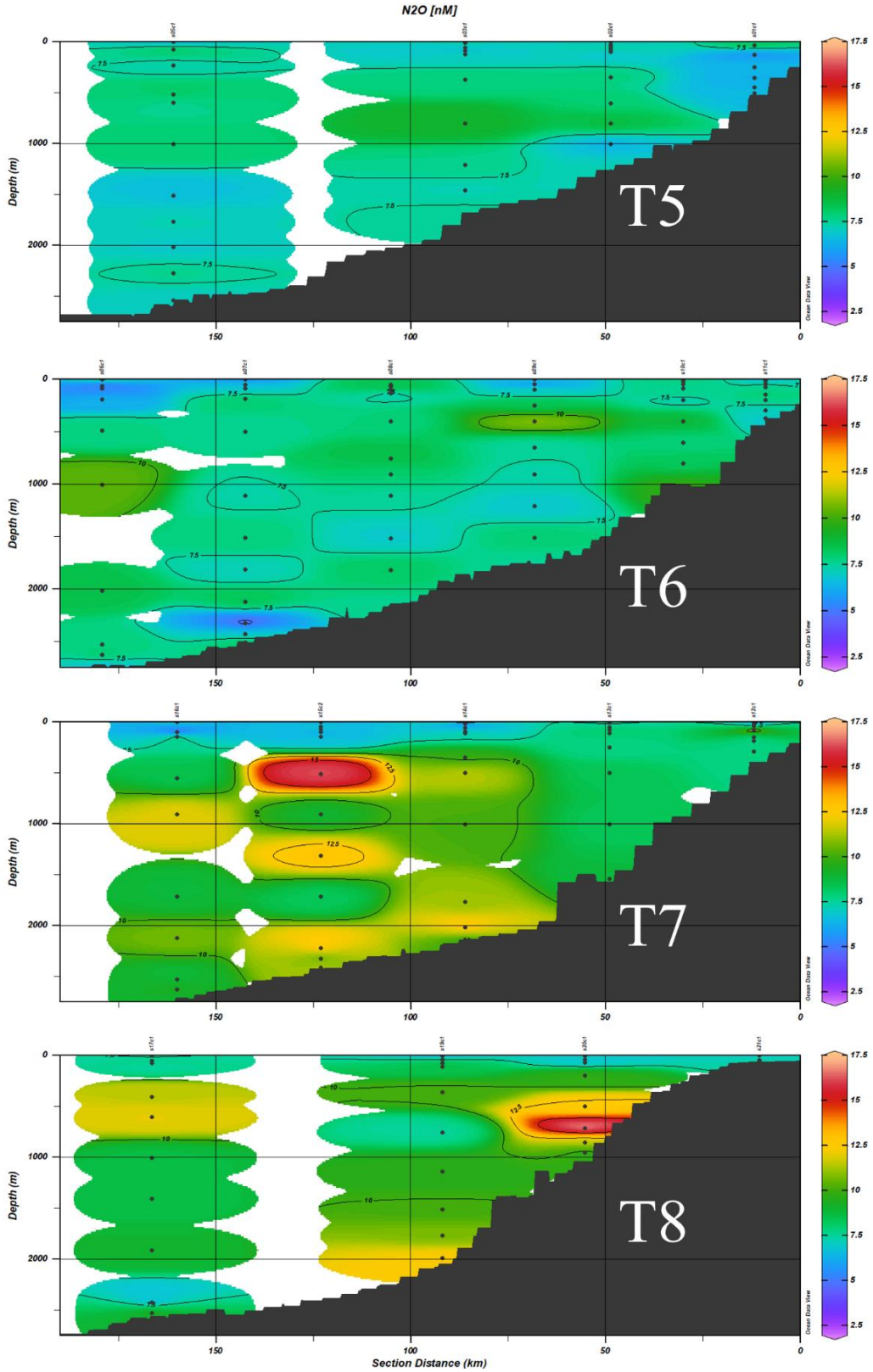

Figure A.25: Schade 2021 N_2O (nM) heat maps. Station labels are on the top axis of each plot and transect labels follow those in Figure 2.1. The black dots represent the location and depth of each data point.

APPENDIX B: OXYGEN MINIMUM ZONE (OMZ) LITERATURE REVIEW

Oxygen (O_2) is a crucial component of oceanic biogeochemistry as it controls the ways in which almost all marine organisms are distributed and interact with each other in the water column. In select areas around the world, there are some points in the water column of low or zero oxygen saturation called oxygen minimum zones (OMZs). OMZs are important because they are integral parts of a regions biogeochemical processes and can control the genetic diversity of organims that have evolved in and around them. OMZs can extend for hundreds of kilometers and can persist permanently in the regions they are found. They are of unique interest to researchers now because of their connection to climate change and their ability to expand under the right conditions.

Previous research done on oxygen minimum zones (OMZs) has revealed much about their biogeochemical relationships and what makes them important. OMZs, oxygen minimum layers, or oxygen-deficient zones can be generally defined as a suboxic layer found between 10-1300 meters deep created when there is high oxygen consumption around the thermocline. This oxygen consumption is the result of microbial respiration of falling organic matter from the euphotic zone. The precise definition of an oxygen minimum zone changes depending on the region that they are found in as there is no one oxygen concentration that defines an OMZ. Some areas define an OMZ by comparing the oxygen saturation percentage of a water body with surface percentages [*Gilly et al.*, 2013]. For example, in the Indian Ocean a water body at a certain depth can be an OMZ if its oxygen content is <10% of sea surface oxygen concentrations. For the Pacific and Indian Oceans, an oxygen concentration of <20 μmol kg^{-1} can qualify a water

body as an OMZ. For the Atlantic Ocean, OMZs are qualified when oxygen concentration is <45 μmol kg^{-1}. OMZs in the open ocean can be found in the Eastern Tropical North Pacific, the Arabian Sea, and off the coast of Peru [*A. Paulmier et al.*, 2006].

OMZs form when oxygenated water moves from the euphotic zone and mixed layer, and into the thermocline and oxygen limited zone (OLZ). The OLZ is the region immediately above or below an OMZ. Here, aerobic bacteria break down the organic matter and oxygen is used in this metabolic process causing the dissolved oxygen concentration in the water column to decrease. Oxygen concentration increases with depth outside the OMZ as the colder water outside of the euphotic zone has higher concentrations of oxygen. Regions like the Eastern South Pacific Ocean has high primary production in the surface ocean as a result of upwelling events near the western coasts of South America. The high primary production results in high oxygen demand due to microbial respiration and, when combined with low ventilation and mixing, an OMZ results [*Fuenzalida et al.*, 2009].

It's important to note that OMZs are not hypoxic "dead zones" like those found in the Gulf of Mexico. Hypoxic areas have an oxygen minimum that occurs on the ocean floor and are not permanent features of the region. OMZS occur at depth ranges within the water column and are permanent features of the regions they are found in due to constant nutrient input from coastal runoff or upwelling [*Gilly et al.*, 2013]. As such they are important because organisms have adapted to live in them and they are a constant addition to the local biogeochemical processes in the area [*Gibson and Atkinson*, 2003; *Mullins et al.*, 1985].

Organisms have adapted to the low oxygen environment in OMZs and thrive in the OLZ [*Gilly et al.*, 2013]. The same idea applies to hypoxic benthos communities. As a result, OMZs

controls the genetic diversity or the organisms that evolved in these regions [*Fuenzalida et al.*, 2009].

Oxygen minimum zones are also important because of their role in the global nitrogen, carbon, and sulfur cycles [*Gilly et al.*, 2013; *Ji et al.*, 2015; *Aurélien Paulmier et al.*, 2011; *Thamdrup et al.*, 2012; *Ward et al.*, 1989]. When looking at a vertical profile of dissolved oxygen and nitrite (NO_2^-) an OMZ/ODZ is characterized by a steep gradient in oxygen concentration trapping an area of significant nitrite accumulation. In OMZs, denitrification, annamox, chemoautotrophic denitrification and sulfate reduction reactions occur as a result of the low oxygen conditions. Above the OMZ, oxygenic photosynthesis, N_2 fixation, aerobic respiration, nitrification, and S oxidation occur. All of these are important for the stability of the biogeochemical systems around the OMZ and some of the them can contribute to the effects of global climate change. Due to the high rates of denitrification and nitrification in and around the OMZ, large amounts of nitrous oxide (a potent greenhouse gas and ozone depletion agent) are produced and can be emitted to the atmosphere [*Ji et al.*, 2015]. High dissolved inorganic carbon (DIC) concentration is associated with OMZs to the point that OMZs can be a sink for carbon. At the same time, bacterial processes in the OMZ can steadily produce carbon dioxide and emit it to the atmosphere [*Aurélien Paulmier et al.*, 2011].

The existence of OMZs has been known for a relatively long time now but within the past two decades research is interested in the relationship between OMZs and climate change. The primary concern about this relationship is if the effects of climate change can affect the extent of an OMZ. OMZs have been shown to change extent naturally over large timescales while variability in surface level productivity and the depth of winter mixing can affect the intensity of the OMZ [*Reichart et al.*, 1998]. Therefore, when predicting the future effects of climate change

on OMZs researchers must also account for any natural variation in the system. Climate change effects can lower ventilation of the water column and O_2 solubility. At the same time natural and anthropogenic fertilization can cause remineralization rates to increase [*Aurélien Paulmier et al.*, 2011]. These possibilities could cause OMZ extent, thickness, and intensity/frequency of its biogeochemical reactions to increase. This results in changes like nitrous oxide production and emissions to the atmosphere increasing and the ecosystem of OLZ and OMZ organisms to change with no clear outcome. Research concerning OMZs is interested in their connection with the effects of climate change. While many studies are being performed to predict future trends, they are working with minimal data collected from research cruises. More time must be spent collecting consistent data from OMZs over a large timescale in order to more accurately assess trends. This is a common problem with most oceanographic research however. For now, research should seek to understand the differences between uniquely located OMZs around the world. Besides upwelling it would be worth noting how regionally specific processes and characteristics can alter the biogeochemistry of an OMZ.